

[Master's Theses](#)

[Master's Theses and Graduate Research](#)

Summer 2018

A Numerical Study of the van Roosbroeck System for Semiconductors

Alan Ghazarians

San Jose State University

Follow this and additional works at: https://scholarworks.sjsu.edu/etd_theses

Recommended Citation

Ghazarians, Alan, "A Numerical Study of the van Roosbroeck System for Semiconductors" (2018).

Master's Theses. 4939.

DOI: <https://doi.org/10.31979/etd.k2yb-6c32>

https://scholarworks.sjsu.edu/etd_theses/4939

A NUMERICAL STUDY OF THE VAN ROOSBROECK SYSTEM FOR
SEMICONDUCTORS

A Thesis
Presented to
The Faculty of the Department of Mathematics
San José State University

In Partial Fulfillment
of the Requirements for the Degree
Master of Science

by
Alan Ghazarians
August 2018

© 2018

Alan Ghazarians

ALL RIGHTS RESERVED

The Designated Thesis Committee Approves the Thesis Titled

A NUMERICAL STUDY OF THE VAN ROOSBROECK SYSTEM FOR
SEMICONDUCTORS

by

Alan Ghazarians

APPROVED FOR THE DEPARTMENT OF MATHEMATICS

SAN JOSÉ STATE UNIVERSITY

August 2018

Daniel Brinkman, Ph.D. Department of Mathematics

Plamen Koev, Ph.D. Department of Mathematics

Mohammad Saleem, Ph.D. Department of Mathematics

ABSTRACT

A NUMERICAL STUDY OF THE VAN ROOSBROECK SYSTEM FOR SEMICONDUCTORS

by Alan Ghazarians

Since the 1950s, semiconductors have played a significant and daily role in our lives, as they are the foundation of our computers, phones, and other electronic devices. Aside from their obvious uses, the equations that govern semiconductors have peaked the interest of mathematicians and numerical analysts. In 1950, van Roosbroeck described the fundamental semiconductor device equations as a system of three nonlinear coupled partial differential equations. The van Roosbroeck system poses a challenge numerically because of its strong nonlinearity and coupled equations. Its difficulties lie in simultaneously solving drift-diffusion equations for electrons and holes and using their solutions to solve the Poisson equation. To start off, we will numerically solve the one-dimensional drift diffusion equation with constant velocity using unwinding techniques and illustrate the results using MATLAB for a toy model. This attempt will only complicate solving two drift-diffusion equations and will not suffice in solving the full van Roosbroeck system. Thus, we will analyze the standard finite difference scheme proposed by Scharfetter and Gummel that deals nicely with the nonlinearity and coupled equations. Then we will compare and contrast the solutions by the standard finite difference scheme proposed by Scharfetter and Gummel and direct discretization of the fluxes in Slotboom variables. We will conclude that the Slotboom discretization performs better than the Scharfetter-Gummel in cases of large forward bias. We will also briefly discuss solar cells and their simulations.

DEDICATION

To my grandfather, Arkadi.

ACKNOWLEDGEMENTS

First and foremost, I would like Professor Daniel Brinkman for your patience and guidance through this nearly yearlong process. I have learned more from this thesis than I have from any other academic project or class. Without a doubt, I have become a better mathematician, programmer, and researcher by working with you. Thank you Professor Plamen Koev and Professor Mohammad Saleem for your numerical linear algebra and numerical analysis courses without which I would not be able to complete this thesis. I would also like to thank Professor Slobodan Simić for the past 7 years of support throughout my academic career. I would not be a mathematician nor have pursued my master's degree without your advice and wisdom. I would also like to thank Professor Fryer, Professor Hsu, and Professor So. Thank you to my lifelong friends, Danny, Danny, and Sato. Thank you to my family Alex, Nicole, Sami, Aida, Jenik, Anita, and Terry. Thank you Mom, Dad, and Milene for always supporting me whether I was living in California, France, or Virginia. Last, but not least, thank you Bella. You are the love of my life and I would not be the person I am today without you.

TABLE OF CONTENTS

CHAPTER

1	INTRODUCTION	1
2	FINITE DIFFERENCE METHODS	6
2.1	Finite Difference Methods Basics	6
2.2	Stability, Convergence, and Consistency	9
2.3	Drift-Diffusion Model	12
2.4	Crank-Nicholson Method	16
2.5	Stability	18
2.6	Velocity as a Potential Vector	20
3	THE VAN ROOSBROECK SYSTEM	25
3.1	The van Roosbroeck System	25
3.2	No Current van Roosbroeck System	28
3.2.1	Constant Current van Roosbroeck System	29
3.2.2	Constant Current with Linear Potential van Roosbroeck System	31
3.3	Gummel Iteration	31
3.4	Damping	33
3.5	Drift-Diffusion in van Roosbroeck System	33
4	SCHARFETTER-GUMMEL SCHEME	36
4.1	Scharfetter-Gummel Discretization	36
4.1.1	Current and Continuity Equations	36
4.1.2	The Poisson Equation	39
4.2	Boundary Conditions	41
4.3	Slotboom Discretization	44
5	SEMICONDUCTOR SIMULATIONS	47
5.1	Generation and Recombination	47
5.2	Shockley-Read-Hall Model	48
5.3	Doping	49
5.4	PN Junction	50
5.5	Depletion Region	50
5.6	External Voltage and Forward/Reverse Bias	51
5.7	Simulation Results	52
5.8	Current-Voltage (IV) Characteristics	58

6	SLOTBOOM AND SCHARFETTER-GUMMEL	76
6.1	Zero Doping	76
6.2	Equal Doping	82
7	SOLAR CELL	89
7.1	Fill Factor	89
7.2	Future Work	91
BIBLIOGRAPHY		92
APPENDIX A (MATLAB Code)		94
A.1	Implicit Drift-Diffusion Equation Solver	94
A.2	Scharfetter-Gummel Finite Difference Scheme	98
A.3	Flux Functions	104
A.4	Solar Cell and Fill Factor	105

LIST OF TABLES

Table

3.1 Parameters and Variables	27
--	----

LIST OF FIGURES

Figure

2.1	Implicit FTBS scheme with a $D = 0.001$ and $v = 2$	14
2.2	Implicit plots of solution as time increases for FTBS	15
2.3	Implicit FTFS scheme with a $D = 0.001$ and $v = -2$	15
2.4	Implicit plots of solution as time increases for FTFS	16
2.5	Crank-Nicholson scheme with $D = 0.001$ and $v = -2$	17
2.6	Crank-Nicholson scheme with $D = 0$ and $v = 0$	18
2.7	Crank-Nicholson scheme with $D = 0.1$ and $v = 0$	18
2.8	Sinusoidal potential ($V = \sin(x)$)	21
2.9	Solution for sinusoidal potential ($V = \sin(x)$)	22
2.10	Sinusoidal potential ($V = -\cos(x)$)	22
2.11	Solution for sinusoidal potential ($V = -\cos(x)$)	23
4.1	Slotboom and Scharfetter-Gummel functions	46
5.1	Electron concentration zero doping	53
5.2	Hole concentration zero doping	54
5.3	Product electron-hole zero doping	55
5.4	Potential zero doping	56
5.5	Density zero doping	56

5.6	Currents zero doping	57
5.7	Current-voltage zero doping	58
5.8	Electron concentration equal doping	59
5.9	Hole concentration equal doping	60
5.10	Product electron-hole equal doping	61
5.11	Potential equal doping	62
5.12	Density equal doping	62
5.13	Currents equal doping	63
5.14	Current-voltage equal doping	64
5.15	Electron concentration higher doping P-type	65
5.16	Hole concentration higher doping P-type	66
5.17	Product electron-hole higher doping P-type	67
5.18	Potential higher doping P-type	68
5.19	Density higher doping P-type	69
5.20	Currents higher doping P-type	70
5.21	Current-voltage higher doping P-type	71
5.22	Electron concentration higher doping N-type	72
5.23	Hole concentration higher doping N-type	72
5.24	Product electron-hole higher doping N-type	73
5.25	Potential higher doping N-type	73
5.26	Density higher doping N-type	74

5.27	Currents higher doping N-type	74
5.28	Current-voltage higher doping N-type	75
6.1	Slotboom zero doping spatial points	77
6.2	Scharfetter-Gummel zero doping spatial points	78
6.3	SG vs. SB zero doping 5 points	79
6.4	SG vs. SB zero doping 20 points	80
6.5	SG vs. SB zero doping 80 points	81
6.6	SG vs. SB zero doping 320 points	82
6.7	Slotboom equal doping spatial points	83
6.8	Scharfetter-Gummel equal doping spatial points	84
6.9	SG vs. SB equal doping 5 points	85
6.10	SG vs. SB equal doping 20 points	86
6.11	SG vs. SB equal doping 80 points	87
6.12	SG vs. SB equal doping 320 points	88
7.1	IV curve and power curve of a solar cell with a shift of 100	90
7.2	IV curve and power curve of a solar cell with a shift of 1000	91

CHAPTER 1

INTRODUCTION

Without mathematics, much of our understanding of the physical world would be nonexistent. Mathematics is vital to the advent of new technologies, which allow us to improve our understanding of the world and each other. While some problems can be solved with pencil, paper, and classical techniques, others require huge amount of computing power and more sophisticated techniques.

That being said, solutions to partial differential equations (PDEs) are an area in which it is necessary to implement these sophisticated techniques. While there are PDEs, such as the wave equation or heat equation, that can be solved analytically, there are other PDEs, such as the infamous Navier-Stokes, which cannot. This paper will explore a system of PDEs with certain conditions that require computers and numerical techniques in order to approximate solutions to the system.

Vasileska and Goodnick [VG06] point out that over the last half of the 20th century, semiconductors continue to play a significant and daily role in everyday life as they are found in computers, phones, televisions, solar cells, and other electronic devices. The development of semiconductor technology is a testament to the collaboration and interactions between physicists, engineers, and mathematicians. While mathematical models allow for predictions otherwise impossible to observe experimentally, numerical simulations have led to more innovative and optimal designs of semiconductor devices without the need to create expensive and time-consuming prototypes.

Everything we see around the world, all matter, is made up of tiny particles

called atoms. Within these atoms, there are three subatomic particles called electrons, protons, and neutrons. Protons and neutrons are of the same size, but protons have a positive charge while neutrons have neutral charge. The electron is about 2000 times smaller than the proton and has a negative charge. Protons and neutrons are at the center of the atom called the nucleus and electrons live in the electron cloud in orbitals surrounding the nucleus. The atomic number is the number of protons in an atom and determines the type of element. Silicon, which will be of relevance throughout this paper, is an element with 14 protons. While silicon has 14 electrons, it has 4 valence electrons meaning that it has 4 electrons in its outermost orbitals and can form 4 covalent bonds with 4 other silicon atoms. When an atom shares its electrons with another atom in order to fill both of their orbitals it creates a covalent bond.

As seen in Silberberg and Amateis [SA15], semiconductors are made from molecules of silicon with a diamond cubic crystal structure. In this structure the atoms are held together by electron-pair bonds formed by electrons in the outermost shell (valence electrons). This structure is very strong and electrically neutral, but one can change the structure by adding impurities, which we will discuss later.

Essential to the theory of semiconductors is the notion that electrons can carry electric current in two different ways. Shockley [Shi50] states that the first is conduction by electrons and the other is conduction by holes. An electron that moves throughout a crystalline structure leaves in its place a hole. Therefore, a hole is not in and of itself a particle, but the empty space once occupied by an electron. Later, we will discuss this movement of electrons and holes in a semiconductor that has elements other than silicon in it.

Semiconductor device modeling started in the 1950s after W.W. van Roosbroeck [vR50] formulated a system of three nonlinear, coupled partial

differential equations known as the fundamental semiconductor equations or van Roosbroeck system while working at Bell Labs in New Jersey. These equations describe the potential distribution, carrier concentrations, and current flow of electrons and holes inside a semiconductor device. Mathematically, these equations consist of a Poisson equation for the electric potential and two drift-diffusion equations for electrons and holes. Described further in Farrell, Rotundo, Doan, Kantner, Fuhrmann, and Koprucki [FRD⁺16], the semiconductor equations are derived from Maxwell's equations, relations from solid-state physics, and knowledge of semiconductors.

In order to understand the difficulty of the van Roosbroeck system, we must mathematically and physically understand each PDE. A PDE is an equation that involves an unknown function of two or more variables and its partial derivatives. A PDE is considered nonlinear because its output is not proportional to its input. According to Evans [Eva15], system of PDEs is considered coupled if the solution to one PDE depends on the solution of another. In the van Roosbroeck system, in order to solve the nonlinear Poisson equation, one must first solve the two drift-diffusion equations. The Poisson equation is the negative Laplacian operator, which takes the second order partial derivative of each variable, equaling some other function ($-\Delta u = f$). For the van Roosbroeck system, the Poisson equation is the negative Laplacian of the electrostatic potential equated to the density of the system. We will see later that we will solve the Poisson equation to obtain the new electrostatic potential at each time step. The drift-diffusion (convection/advection-diffusion) equation ($u_t = au_x + bu_{xx}$) is a combination two PDEs: the drift (advection) equation ($u_t = au_x$) and the diffusion (heat) equation ($u_t = au_{xx}$). LeVeque [Lev07] states that the drift equation describes the transport of a substance over time while the diffusion equation describes the distribution of a

substance over time. Farrell, Rotundo, Doan, Kantner, Fuhrmann, and Koprucki [FRD⁺16] state that the two drift-diffusion equations describe the drift of electrons and holes throughout a semiconductor and the diffusion of electrons and holes across the PN junction of a semiconductor. Hence, the drift-diffusion equations describe the current flow in semiconductors.

Aside from the practical uses of semiconductors, the equations that govern semiconductors have peaked the interest of mathematicians and numerical analysts according to Markowich [Mar86]. In the 1970s, mathematicians focused on proving existence and uniqueness of solutions using theories of partial differential equations for the van Roosbroeck system. The increased interest from a mathematical perspective and the physical understanding of the system led to a development of better numerical techniques. This interaction between mathematics and physics allowed analysis and simulation of more complicated, multidimensional devices.

Sometimes, analytically solving a system of PDEs becomes too difficult as is the case of the Navier-Stokes equations for incompressible, viscous flow. In these situations, mathematicians and numerical analysts implement numerical techniques such as finite difference, finite element, or finite volume methods in order to approximate solutions. Finite difference methods usually yield solutions that are just as accurate and useful as analytic solutions. Of course, finite difference methods are not restricted to solving PDEs that have no analytic solution. In fact, these methods can give insight and provide efficient solutions to PDEs. Finite difference methods assume a grid upon which the derivatives of the PDE are approximated using a stencil or molecule. Then, in order to approximate the solution at other points in space, the stencil moves throughout the grid as explained by Smith [Smi73].

In the beginning stages of semiconductor device modeling, simplified

one-dimensional models were easily solved analytically, which gave insight and understanding to improve their designs. As the devices became bigger and more complicated, numerical simulation techniques such as finite difference methods were implemented in order to model these devices and create better ones. Soon after, it was realized that standard finite difference methods and discretizations were no longer appropriate as they required massive amounts of computational power and storage. The complications lie in the nonlinearities and coupling of the system itself, so there was a need for a method that could deal with the nonlinearities and coupling. Selberherr [Sel84] describes that these issues were overcome in the 1960s when Scharfetter and Gummel created a nonstandard way of discretizing the van Roosbroeck system.

CHAPTER 2

FINITE DIFFERENCE METHODS

In this chapter we will review the basics of finite difference methods, their stability, convergence, and consistency, and provide examples of solutions to different PDEs.

2.1 Finite Difference Methods Basics

The one-dimensional heat equation with homogenous Dirichlet boundary conditions given by

$$\begin{cases} u_t = u_{xx} \\ u(0, t) = u(L, t) \\ u(x, 0) = f(x) \end{cases} \quad (2.1)$$

has a well-known analytical solution found by using separation of variables as shown in Burden and Faires [BF11], Evans [Eva15], Larsson and Thomée [LT09], and LeVeque [Lev07]. The solution is

$$u(x, t) = \sum_{n=1}^{\infty} c_n \sin\left(\frac{n\pi x}{L}\right) \exp\left(-\frac{n^2\pi^2 t}{L^2}\right) \quad (2.2)$$

where

$$c_n = \frac{2}{L} \int_0^L f(x) \sin\left(\frac{n\pi x}{L}\right) dx. \quad (2.3)$$

Smith [Smi73] points out that an analytical solution is hard to come by with most PDEs, so using numerical techniques become necessary. First, we will work on a uniform grid where the spatial steps are given by $x_{i+1} = x_i + i\Delta x$ and the temporal steps are given by $t_j = t_j + j\Delta t$. The goal of finite difference methods is to solve the PDE on the entire grid as we approach a steady-state solution.

We now introduce finite difference methods, which use the approximation of the derivative found using a Taylor series expansion of $f(x + \Delta x)$. Some approximations are given by the following:

$$f'(x) \approx \frac{f(x + \Delta x) - f(x)}{\Delta x} + \mathcal{O}(\Delta x) \quad (2.4)$$

and

$$f'(x) \approx \frac{f(x) - f(x - \Delta x)}{\Delta x} + \mathcal{O}(\Delta x) \quad (2.5)$$

and

$$f'(x) \approx \frac{f(x + \Delta x) - f(x - \Delta x)}{2\Delta x} + \mathcal{O}(\Delta x^2). \quad (2.6)$$

In Larsson and Thomée [LT09], these approximations are known as forward, backward, and central difference formulas, respectively.

We will use the forward difference formula to approximate the value of the function at a specified grid point x_i as

$$f'(x_i) \approx \frac{f(x_i + \Delta x) - f(x_i)}{\Delta x} = \frac{f(x_{i+1}) - f(x_i)}{\Delta x}. \quad (2.7)$$

With the heat equation, we have a derivative with respect to time and space, so we will need to approximate our derivatives at points (x_i, t_j) using forward differences. We will denote our approximations as

$$u_t(x_i, t_j) = \frac{\partial u}{\partial t} \Big|_{(x_i, t_j)} = \frac{u_{i,j+1} - u_{i,j}}{\Delta t} \quad (2.8)$$

$$u_{xx}(x_i, t_j) = \frac{\partial^2 u}{\partial x^2} \Big|_{(x_i, t_j)} = \frac{u_{i+1,j} - 2u_{i,j} + u_{i-1,j}}{\Delta x^2}. \quad (2.9)$$

Using these approximations, we can write the heat equation as follows:

$$u_{i,j+1} = Ru_{i+1,j} + (1 - 2R)u_{i,j} + Ru_{i-1,j} \quad (2.10)$$

$$\text{where } R = \frac{\Delta t}{\Delta x^2}.$$

This finite difference method is considered an explicit scheme, which means we use the previous time solution to approximate the future time solution. We can also use an implicit scheme given by

$$u_{i,j} = -Ru_{i+1,j+1} + (1 + 2R)u_{i,j+1} - Ru_{i-1,j+1}. \quad (2.11)$$

The explicit and implicit finite difference schemes can now be thought of as a system of equations and, therefore, solved by using a matrix equation given by

$$\vec{u}^{j+1} = A\vec{u}^j \quad (2.12)$$

where

$$A = \begin{bmatrix} 1 - 2R & R & 0 & \dots & \dots & 0 & 0 \\ R & 1 - 2R & R & 0 & \dots & \dots & 0 \\ 0 & R & 1 - 2R & R & \ddots & & \vdots \\ \vdots & \ddots & R & \ddots & \ddots & \ddots & \vdots \\ \vdots & & \ddots & \ddots & \ddots & \ddots & 0 \\ 0 & & & \ddots & \ddots & \ddots & R \\ 0 & 0 & \dots & \dots & 0 & R & 1 - 2R \end{bmatrix}. \quad (2.13)$$

In the case of the implicit finite difference scheme, we are solving

$$\vec{w}^j = B\vec{w}^{j+1} \quad (2.14)$$

where

$$B = \begin{bmatrix} 1 + 2R & -R & 0 & \dots & \dots & 0 & 0 \\ -R & 1 + 2R & -R & 0 & \dots & \dots & 0 \\ 0 & -R & 1 + 2R & -R & \ddots & & \vdots \\ \vdots & \ddots & -R & \ddots & \ddots & \ddots & \vdots \\ \vdots & & \ddots & \ddots & \ddots & \ddots & 0 \\ 0 & & & \ddots & \ddots & \ddots & -R \\ 0 & 0 & \dots & \dots & 0 & -R & 1 + 2R \end{bmatrix}. \quad (2.15)$$

2.2 Stability, Convergence, and Consistency

When using a finite difference scheme, we are concerned with the conditions for which the scheme will yield reasonably accurate approximations to the solution of the PDE. According to Smith [Smi73], in order to determine whether or not a finite difference scheme approximates the solution, we look at the stability, convergence, and consistency. We will denote the exact analytical solution to a PDE as $u(x, t)$ and the computed solution from the finite difference scheme as $u_{i,j}$.

O'Brien and Kaplan [BK50] state say that a finite difference scheme is stable if the computed solution remains finite ($|u_{i,j}| < \infty$) and does not oscillate unnecessarily as $\Delta x, \Delta t \rightarrow 0$. The most common procedure to check for stability is called von Neumann stability analysis in which we assume that the solution is a finite Fourier series. We denote the solution as $u_{p,q} = \xi^q e^{i\beta ph}$ where ξ is known as the amplification factor. In order for our finite difference scheme to be stable, we must have $|\xi| \leq 1$.

Performing a von Neumann stability analysis on the explicit scheme for the heat equation derived above looks like

$$\xi^{q+1} e^{i\beta ph} = R\xi^q e^{i\beta(p+1)h} + (1 - 2R)\xi^q e^{i\beta ph} + R\xi^q e^{i\beta(p-1)h} \quad (2.16)$$

$$\xi = 2 \cos(\beta h) + (1 - 2R), \quad (2.17)$$

which yields the well-known condition that $0 \leq R \leq \frac{1}{2}$.

While the explicit scheme is easy to derive and use, it, unfortunately, only provides accurate solutions for $0 < R \leq \frac{1}{2}$ as found above. Instead of using an explicit scheme, we can use an implicit time scheme given by:

$$u_{i,j} = -Ru_{i-1,j+1} + (1 + 2R)u_{i,j+1} - Ru_{i-1,j+1}. \quad (2.18)$$

After performing a von Neumann stability analysis, we can see that implicit scheme is unconditionally stable unlike the explicit scheme. In order to assess the stability of a finite difference method, one can also use matrix norms or Gershgorin circles as further explained in Smith [Smi73].

While having a finite difference scheme be stable is desirable, we also want it to converge to the actual solution. We say that a finite difference scheme is convergent if the computed solution and the exact analytic solution coincide at a point at the space and time step go to 0:

$$\lim_{\Delta x, \Delta t \rightarrow 0} |u(x, t) - u_{i,j}| \rightarrow 0. \quad (2.19)$$

In general, determining whether a finite difference scheme is convergent is quite difficult because we are usually trying to approximate a solution to a PDE whose analytical solution does not exist (i.e. Navier-Stokes). We will discuss briefly that

the convergent criteria can be determined albeit an analytical solution does not exist.

Another useful measure of whether the finite difference scheme is good or not is consistency. In order to determine consistency of a finite difference scheme, we need to calculate the local truncation error, $T_{i,j}$, which is the amount by which the exact solution fails to satisfy the difference equation. In order to calculate $T_{i,j}$, one uses the Taylor expansions of the terms in the finite difference scheme. Thus,

$$T_{i,j} = \frac{u_{i,j+1} - u_{i,j}}{\Delta t} - \frac{u_{i+1,j} - 2u_{i,j} + u_{i-1,j}}{\Delta x^2} \quad (2.20)$$

where

$$u_{i,j+1} = u_{i,j} + \Delta t \frac{\partial u}{\partial t} + \frac{1}{2!} \Delta t^2 \frac{\partial^2 u}{\partial t^2} + \frac{1}{3!} \Delta t^3 \frac{\partial^3 u}{\partial t^3} + \dots, \quad (2.21)$$

$$u_{i+1,j} = u_{i,j} + \Delta x \frac{\partial u}{\partial x} + \frac{1}{2!} \Delta x^2 \frac{\partial^2 u}{\partial x^2} + \frac{1}{3!} \Delta x^3 \frac{\partial^3 u}{\partial x^3} \dots, \quad (2.22)$$

$$u_{i-1,j} = u_{i,j} - \Delta x \frac{\partial u}{\partial x} + \frac{1}{2!} \Delta x^2 \frac{\partial^2 u}{\partial x^2} - \frac{1}{3!} \Delta x^3 \frac{\partial^3 u}{\partial x^3} \dots. \quad (2.23)$$

In general, finding $T_{i,j}$ is tedious, so we will gloss over the calculation and simply state that for the explicit scheme of the heat equation is

$$T_{i,j} = \frac{1}{2} \Delta t \frac{\partial^2 u}{\partial t^2} - \frac{1}{12} \Delta x^2 \frac{\partial^4 u}{\partial x^4}, \quad (2.24)$$

which can also be stated as

$$T_{i,j} = \mathcal{O}(\Delta t) + \mathcal{O}(\Delta x^2). \quad (2.25)$$

A finite difference scheme is called consistent if

$$\lim_{\Delta x, \Delta t \rightarrow 0} T_{i,j} \rightarrow 0. \quad (2.26)$$

We can see that the explicit finite difference scheme for the heat equation is consistent.

An important theorem which relates stability, convergence, and consistency of a finite difference scheme is called Lax's Equivalence Theorem. The theorem states that for a given properly posed linear initial value problem, a linear finite difference scheme that is stable and consistent is also convergent. For a detailed and complete proof of Lax's Equivalence theorem, refer to Lax and Richtmyer [LR56] and Richtmyer and Morton [RDM55]. The explicit finite difference scheme is stable under certain conditions, consistent, and therefore, convergent by Lax's Equivalence theorem.

For our future finite difference schemes, we will use implicit schemes. According to Ascher, Ruuth, and Spiteri [ARS97], although implicit schemes are more complex to implement and require more computational effort in each step, we can use bigger time steps. That is, they are stable without having to take the time step to be very small unlike an explicit scheme.

2.3 Drift-Diffusion Model

Now we look at a drift-diffusion equation and its initial value problem on the interval $[0, L]$ given by

$$\begin{cases} u_t = Du_{xx} - vu_x \\ u(0, t) = u(L, t), u_x(0, t) = u_x(L, t) \\ u(x, 0) = f(x) \end{cases} \quad (2.27)$$

where D is the diffusion coefficient and v is the velocity. Note that the drift-diffusion equation is a combination of a parabolic and hyperbolic PDE. We discretize the drift-diffusion equation on a uniform grid with intervals $[x_i, x_{i+1}]$ for $i = 0, 1, 2, \dots, N$ by employing a standard implicit forward time forward space (FTFS) finite difference scheme to obtain the following:

$$\frac{u_i^{n+1} - u_i^n}{\Delta t} = D \left(\frac{u_{i+1}^{n+1} - 2u_i^{n+1} + u_{i-1}^{n+1}}{\Delta x^2} \right) - v \left(\frac{u_{i+1}^{n+1} - u_i^{n+1}}{\Delta x} \right). \quad (2.28)$$

Letting $R_1 = \frac{\Delta t}{\Delta x}$ and $R_2 = \frac{\Delta t}{\Delta x^2}$ we can write the above as:

$$u_i^n = u_{i+1}^{n+1}(vR_1 - DR_2) + u_i^{n+1}(1 + 2DR_2 - vR_1) + u_{i-1}^{n+1}(-DR_2). \quad (2.29)$$

Similarly, we can use an implicit forward time backward space (FTBS) finite difference scheme to obtain:

$$\frac{u_i^{n+1} - u_i^n}{\Delta t} = D \left(\frac{u_{i+1}^{n+1} - 2u_i^{n+1} + u_{i-1}^{n+1}}{\Delta x^2} \right) - v \left(\frac{u_i^{n+1} - u_{i-1}^{n+1}}{\Delta x} \right). \quad (2.30)$$

Subsequently, we would have

$$u_i^n = u_{i+1}^{n+1}(-DR_2) + u_i^{n+1}(1 + 2DR_2 + vR_1) + u_{i-1}^{n+1}(-DR_2 - vR_1). \quad (2.31)$$

We can write our implicit FTBS finite difference scheme as

$$\vec{u}^n = A \vec{u}^{n+1} \quad (2.32)$$

where

$$A = \begin{bmatrix} \lambda_1 & \lambda_2 & 0 & \dots & \dots & 0 & \lambda_3 \\ \lambda_3 & \lambda_1 & \lambda_2 & 0 & \dots & \dots & 0 \\ 0 & \lambda_3 & \lambda_1 & \lambda_2 & \ddots & & \vdots \\ \vdots & \ddots & \lambda_3 & \ddots & \ddots & \ddots & \vdots \\ \vdots & & \ddots & \ddots & \ddots & \ddots & 0 \\ 0 & & & \ddots & \ddots & \ddots & \lambda_2 \\ \lambda_2 & 0 & \dots & \dots & 0 & \lambda_3 & \lambda_1 \end{bmatrix} \quad (2.33)$$

where $\lambda_1 = 1 + DR_2 + vR_1$, $\lambda_2 = -DR_2$, and $\lambda_3 = -DR_2 - vR_1$.

For the implicit FTFS finite difference scheme we have the same matrix, but $\lambda_1 = 1 + DR_2 - vR_1$, $\lambda_2 = vR_1 - DR_2$, and $\lambda_3 = -DR_2$.

The results for the drift-diffusion initial value problem are illustrated in Figures 2.1-2.4. In the figures, we can see both the drift and diffusion of our initial condition, which, in this case, is a Gaussian centered at the midpoint of the interval $[0, L]$.

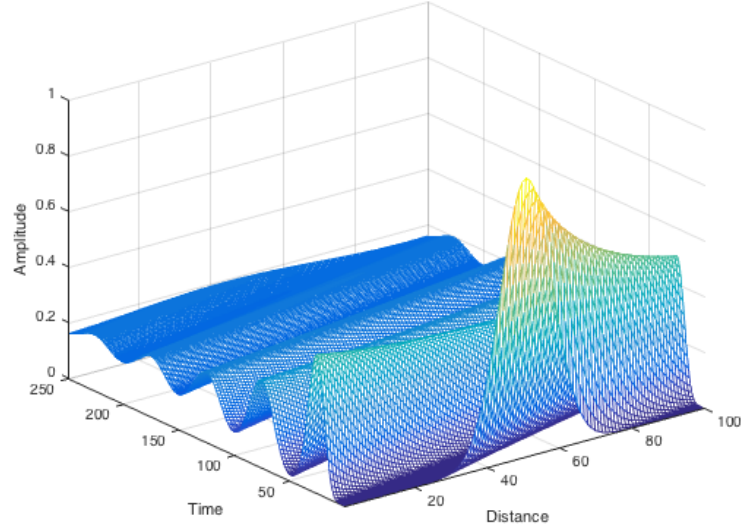


Figure 2.1: Implicit FTBS scheme with a $D = 0.001$ and $v = 2$.

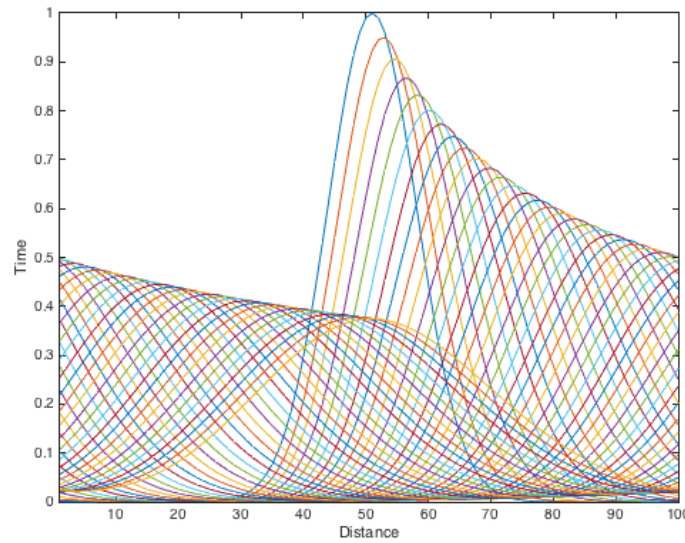


Figure 2.2: Implicit plots of solution as time increases for FTBS.

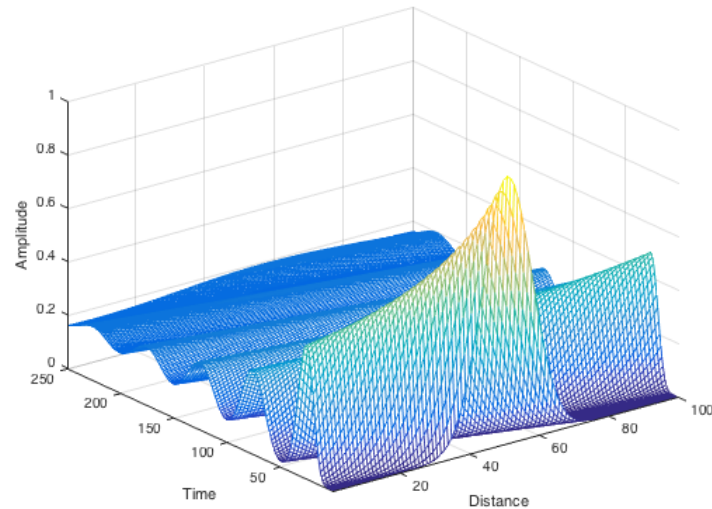


Figure 2.3: Implicit FTFS scheme with a $D = 0.001$ and $v = -2$.

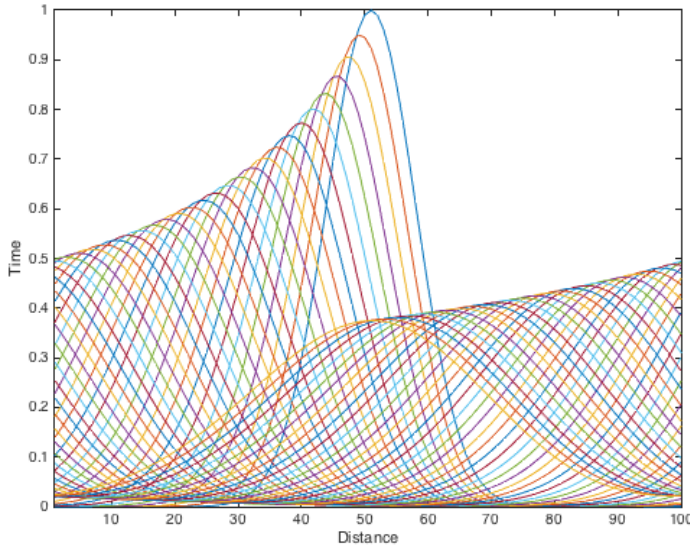


Figure 2.4: Implicit plots of solution as time increases for FTFS.

2.4 Crank-Nicholson Method

Normally, one would try to employ an explicit finite difference scheme to a PDE, however, issues of stability, convergence, and truncation errors arise with respect to the temporal and spatial step sizes. Instead of using an explicit scheme, we will focus on using implicit schemes, however, the implicit FTFS and FTBS finite difference methods are not the only implicit finite difference methods that we can employ to solve the drift-diffusion equation. In fact, another popular implicit method is the Crank-Nicholson method created by Crank and Nicolson [CN47] in 1947, which is unconditionally stable, convergent, and has a small truncation error. The Crank-Nicholson finite difference method makes use of the midpoint between two time steps. The Crank-Nicholson finite difference method for the drift-diffusion equation is as follows:

$$\frac{u_i^{n+1} - u_i^n}{\Delta t} = \frac{D}{2} \left(\frac{u_{i+1}^{n+1} - 2u_i^{n+1} + u_{i-1}^{n+1}}{\Delta x^2} + \frac{u_{i+1}^n - 2u_i^n + u_{i-1}^n}{\Delta x^2} \right) - \frac{v}{2} \left(\frac{u_{i+1}^{n+1} - u_i^{n+1}}{\Delta x} + \frac{u_{i+1}^n - u_i^n}{\Delta x} \right). \quad (2.34)$$

Figures 2.5-2.7 show the solutions to the drift-diffusion equation using the Crank-Nicolson finite difference method for different values of diffusion and velocity.

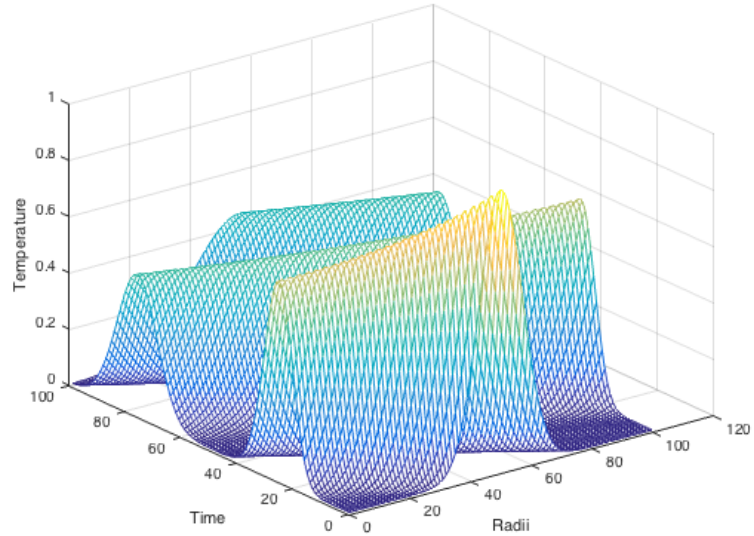


Figure 2.5: Crank-Nicholson scheme with $D = 0.001$ and $v = -2$.

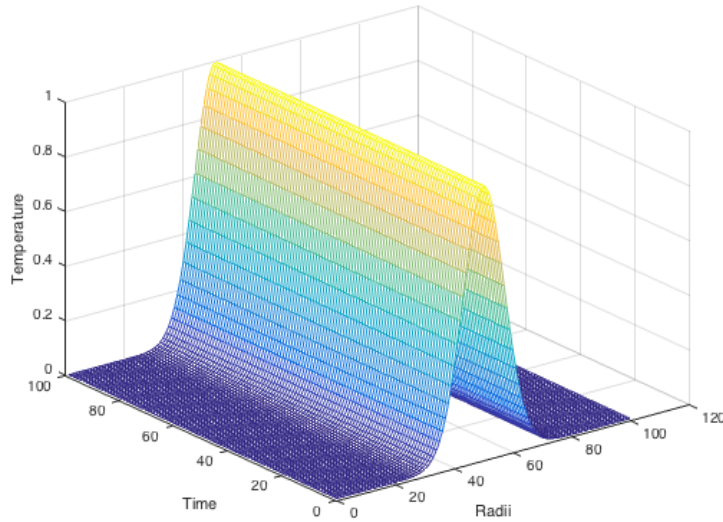


Figure 2.6: Crank-Nicholson scheme with $D = 0$ and $v = 0$.

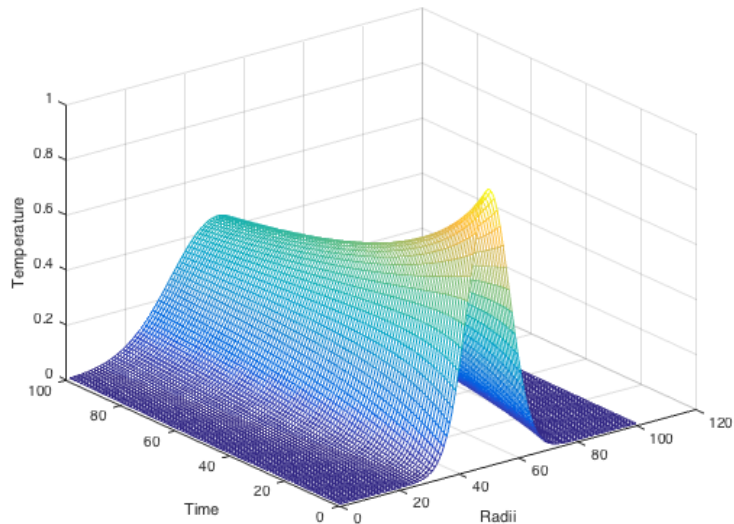


Figure 2.7: Crank-Nicholson scheme with $D = 0.1$ and $v = 0$.

2.5 Stability

Previously we considered both a forward space and backward space finite difference scheme. When plotting the results of the system we chose our velocity v ,

spatial, and temporal step carefully in order for the scheme to be stable. However, once we start simulating semiconductor devices, we will not have the liberty to chose our parameters in order to ensure stability. We will have to adhere to physical limitations and constraints such as the length of a typical semiconductor device or the total time of simulation. As described in LeVeque [Lev07], we perform a von Neumann stability analysis with $u_p^q = \xi^q e^{i\beta ph}$ to determine when our FTFS and FTBS finite difference schemes are stable.

For the implicit FTFS finite difference scheme we obtain the following:

$$\xi^{q+1} e^{i\beta ph} - \xi^q e^{i\beta ph} = DR_2(\xi^{q+1} e^{i\beta(p+1)h} - 2\xi^{q+1} e^{i\beta ph} + \xi^{q+1} e^{i\beta(p-1)h}) - vR_1(\xi^{q+1} e^{i\beta(p+1)h} - \xi^{q+1} e^{i\beta ph}). \quad (2.35)$$

After solving for ξ we obtain:

$$\xi = \frac{1}{1 + (4DR_2 - 2vR_1) \sin^2(\frac{\beta h}{2}) + 2ivR_1 \sin(\beta h)} \quad (2.36)$$

and

$$\xi = \frac{1}{1 + (4DR_2 + 2vR_1) \sin^2(\frac{\beta h}{2}) + 2ivR_1 \sin(\beta h)} \quad (2.37)$$

for the FTFS and FTBS, respectively.

In order for our scheme to be stable we need

$$|\xi|^2 = \frac{1}{\left(1 + (4DR_2 \mp 2vR_1) \sin^2(\frac{\beta h}{2})\right)^2 + \left(2vR_1 \sin(\beta h)\right)^2} \leq 1. \quad (2.38)$$

We can see that for $D > 0$, $R_1 > 0$, $R_2 > 0$, the FTFS finite difference scheme is stable when $v < 0$ and the FTBS finite difference scheme is stable when $v > 0$. This justifies our carefully picked v in the previous section when solving the

drift-diffusion system. The stability analysis means that we must implement the following upwinding scheme for our finite difference scheme to be stable:

$$\frac{u_i^{n+1} - u_i^n}{\Delta t} = D \left(\frac{u_{i+1}^{n+1} - 2u_i^{n+1} + u_{i-1}^{n+1}}{\Delta x^2} \right) - v \left(\frac{u_{i+1}^{n+1} - u_i^{n+1}}{\Delta x} \right), v < 0 \quad (2.39)$$

and

$$\frac{u_i^{n+1} - u_i^n}{\Delta t} = D \left(\frac{u_{i+1}^{n+1} - 2u_i^{n+1} + u_{i-1}^{n+1}}{\Delta x^2} \right) - v \left(\frac{u_i^{n+1} - u_{i-1}^{n+1}}{\Delta x} \right), v > 0. \quad (2.40)$$

2.6 Velocity as a Potential Vector

Up until now, we have assumed that our velocity v is a constant, however, this is not always the case. In fact, for most semiconductor device modeling we will want to define our velocity as a potential: $v = -\nabla V$. Using this definition we will have to use our upwinding scheme. That is, we must choose to either use a FTFS or FTBS finite difference scheme depending on the sign of v at each spatial grid point. We will consider two types of potentials: linear and sinusoidal.

For the linear potential $V = ax + b$ where $a, b \in \mathbb{R}$ and $a \neq 0$. We can see that our velocity is constant at all grid points given a linear potential in x . Thus, we expect to get the same results as the implicit FTFS or FTBS finite difference scheme depending on whether velocity is positive or negative, respectively. That is, our upwinding scheme works. Hence, for a linear potential (constant velocity) our upwinding scheme performs as we would expect. In fact, the results are exactly the same as the results for the drift-diffusion initial value problem explain in Section 2.3.

For a sinusoidal potential $V = \sin(x)$ or $V(x) = \cos(x)$ we define our velocity using a forward scheme, which gives us the following:

$$v = -\nabla V = -\frac{V_{i+1} - Vi}{\Delta x} = -\frac{\sin(x_{i+1}) - \sin(x_i)}{\Delta x}. \quad (2.41)$$

Figures 2.8-2.11 show the solutions to the drift-diffusion equation using a finite difference method for sinusoidal potentials.

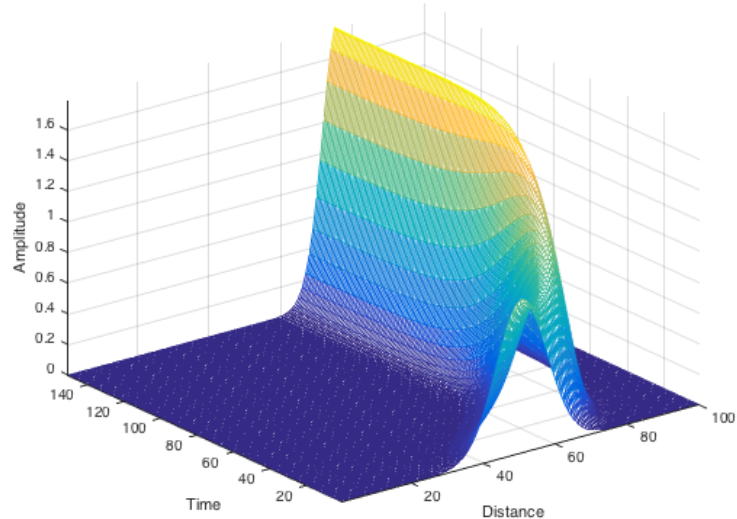


Figure 2.8: Sinusoidal potential ($V = \sin(x)$).

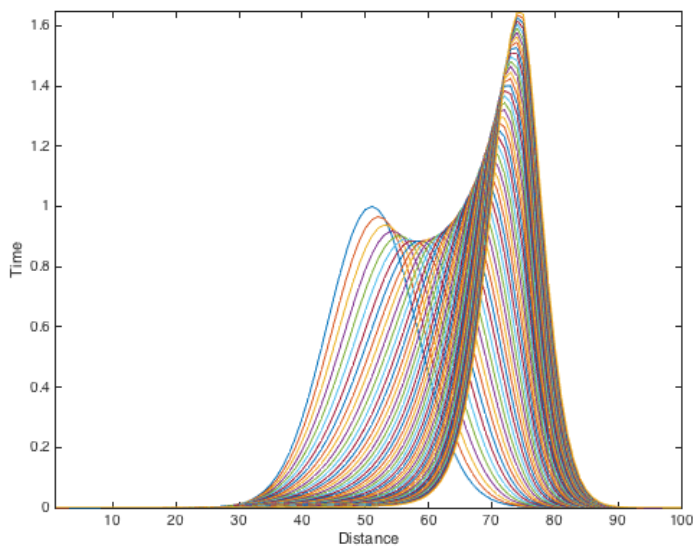


Figure 2.9: Implicit solution as time increases for a sinusoidal potential ($V = \sin(x)$).

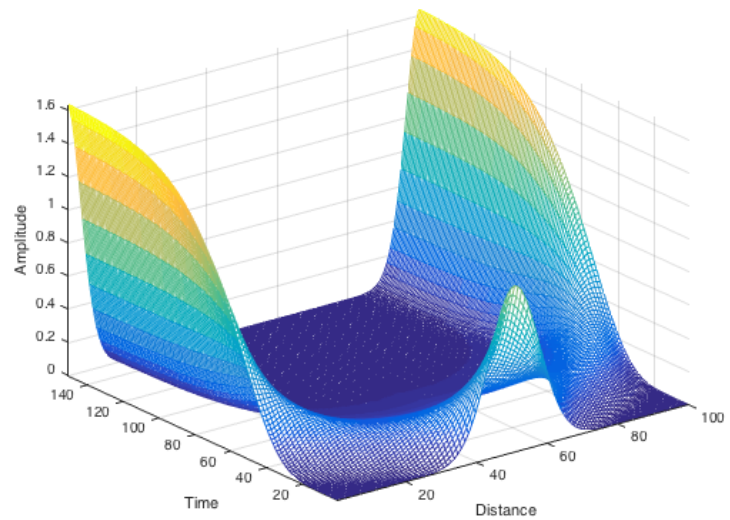


Figure 2.10: Sinusoidal potential ($V = -\cos(x)$).

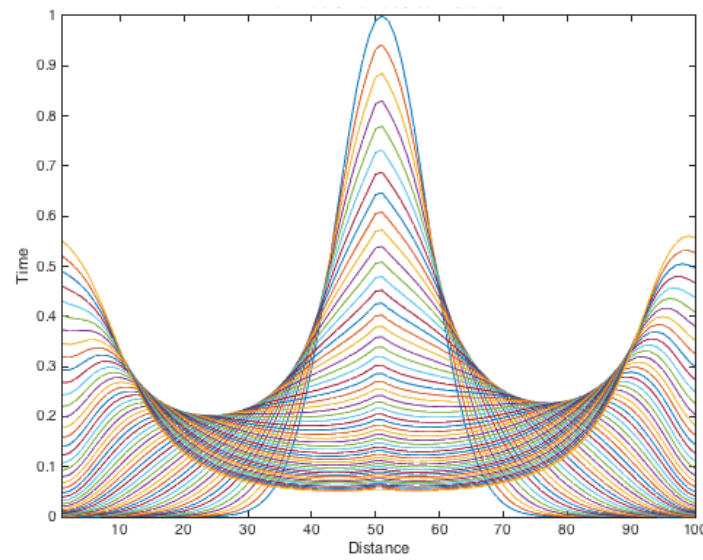


Figure 2.11: Implicit solution as time increases for sinusoidal potential ($V = -\cos(x)$)

Note that for the sinusoidal potentials, our solution converges to a steady state solution. We confirm this by seeing that as $n \rightarrow \infty$

$$\|u^{n+1} - u^n\| \rightarrow 0 \quad (2.42)$$

for some norm $\|\cdot\|$. Thus, we can say that as $n \rightarrow \infty$ our numerical solution converges to some refined solution u^N .

Although the MATLAB code can account for the change of signs of the velocity at each gridpoint, it becomes tedious and unnecessary. We will see that the upwinding scheme can be replaced by the more commonly used Scharfetter-Gummel finite difference scheme. Before we deriving this scheme, we will introduce the van Roosbroeck system.

CHAPTER 3

THE VAN ROOSBROECK SYSTEM

In order to understand and analyze semiconductor structure, we must have a mathematical model. This model, as stated earlier, can be derived from Maxwell's equations, solid-state physics, and some other assumptions. For a full derivation of the semiconductor equations, refer to Selberherr [Sel84], van Roosbroeck [vR50], or Vasileska and Goodnick [VG06]. However, the focus of this paper lies in the numerical methods used to solve the van Roosbroeck system and not the physics behind these equations.

3.1 The van Roosbroeck System

The drift-diffusion system, also known as the van Roosbroeck system, consists of three nonlinear partial differential equations given by:

$$J_n = q\mu_n n E + qD_n \nabla n \quad (3.1)$$

$$J_p = q\mu_p p E - qD_p \nabla p \quad (3.2)$$

$$\frac{\partial n}{\partial t} = \frac{1}{q} \nabla \cdot J_n + R \quad (3.3)$$

$$\frac{\partial p}{\partial t} = -\frac{1}{q} \nabla \cdot J_p + R \quad (3.4)$$

$$-\nabla \cdot \epsilon \nabla V = q(p - n + C) \quad (3.5)$$

where $E = -\nabla V$.

For our purposes, we will only focus on and solve the one-dimensional system given by current equations,

$$J_n = q\mu_n nE + qD_n \frac{dn}{dx} \quad (3.6)$$

$$J_p = q\mu_p pE - qD_p \frac{dp}{dx}, \quad (3.7)$$

continuity equations,

$$\frac{dn}{dt} = \frac{1}{q} \frac{dJ_n}{dx} + R \quad (3.8)$$

$$\frac{dp}{dt} = -\frac{1}{q} \frac{dJ_p}{dx} + R, \quad (3.9)$$

and the Poisson equation,

$$-\varepsilon \frac{d^2V}{dx^2} = q(p - n + C) \quad (3.10)$$

where $E = -\frac{dV}{dx}$ and the subscripts n and p represent electrons and holes, respectively. If the current equations are plugged into the continuity equations, we can see that the van Roosbroeck system consists of two drift-diffusion equations and a Poisson equation. The drift-diffusion equations describe the drift and diffusion of the concentrations of electrons and holes throughout a semiconductor due to the electric field. The Poisson equation relates the electrostatic potential to a given charge distribution. Table 3.1 shows the description of all the parameters and variables used in the van Roosbroeck system.

Table 3.1: Description of Parameters and Variables in van Roosbroeck system.

Name	Symbol	Value	Units
Electron concentration	n		$\frac{1}{m^3}$
Hole concentration	p		$\frac{1}{m^3}$
Electron current density	J_n		$\frac{A}{m^2}$
Hole current density	J_p		$\frac{A}{m^2}$
Doping concentration	C		$\frac{1}{m^3}$
Reaction term	R		$\frac{1}{m^3 s}$
Electrostatic potential	V		V
Electron diffusion coefficient	D_n		$\frac{m^2}{s}$
Hole diffusion coefficient	D_p		$\frac{m^2}{s}$
Electron mobility	μ_n	0.14	$\frac{m^2}{Vs}$
Hole mobility	μ_p	0.045	$\frac{m^2}{Vs}$
Permittivity of free space	ε_0	$8.854187817 * 10^{-12}$	$\frac{s^4 A^2}{m^3 kg}$
Dielectric constant silicon	ε_{Si}	11.68	dimensionless
Permittivity of silicon	ε	$\varepsilon_0 * \varepsilon_{Si}$	$\frac{s^4 A^2}{m^3 kg}$
Boltzmann constant	k_B	$1.38064852 * 10^{-23}$	$\frac{m^2 kg}{K s^2}$
Elementary charge	q	$1.602 * 10^{-19}$	C
Temperature	T	300	K
Thermal voltage	$V_T = \frac{k_B T}{q}$	0.025854841198502	V
Intrinsic concentration	n_{int}	$1.5 * 10^{16}$	$\frac{1}{m^3}$

3.2 No Current van Roosbroeck System

In some cases, we can solve the drift-diffusion equations analytically for n and p . One special case is when there is no current for either electrons nor holes ($J_p = J_n = 0$) with initial conditions $n(0) = n_{int}$ and $p(0) = n_{int}$ and a given potential V . The current equation for electrons becomes

$$J_n = -q\mu_n n \frac{dV}{dx} + qD_n \frac{dn}{dx} = 0 \quad (3.11)$$

thus,

$$\frac{dn}{dx} = \frac{\mu_n n}{D_n} \frac{dV}{dx}. \quad (3.12)$$

Using Einstein's relation $\frac{D}{\mu} = \frac{k_B T}{q}$, we arrive at

$$\frac{dn}{dx} = \frac{nq}{k_B T} \frac{dV}{dx} \quad (3.13)$$

which is a ordinary differential equation along with the initial condition that can be easily solved as

$$n = n_{int} \exp \left(\frac{q(V - V_n)}{k_B T} \right). \quad (3.14)$$

Similarly, for the holes the solution will be

$$p = n_{int} \exp \left(\frac{-q(V - V_p)}{k_B T} \right) \quad (3.15)$$

where $V_n = V_p = V_0$ are initial potentials for electrons and holes, respectively.

Note that we have the following:

$$n \cdot p = n_{int} \exp \left(\frac{q(V - V_0)}{k_B T} \right) \cdot n_{int} \exp \left(\frac{-q(V - V_0)}{k_B T} \right) = n_{int}^2. \quad (3.16)$$

Vasileska and Goodnick [VG06] state that the solutions to the zero current problem are often called the Quasi-Fermi level variables denoted by:

$$n = n_{int} \exp \left(\frac{q(V - V_n)}{k_B T} \right) \quad (3.17)$$

$$p = n_{int} \exp \left(\frac{-q(V - V_p)}{k_B T} \right). \quad (3.18)$$

We can reformulate our solutions by using the Slotboom variables formulated by Slotboom [Slo73], which are defined as:

$$\Phi_n = n_{int} \exp \left(\frac{-qV_n}{k_B T} \right) \quad (3.19)$$

$$\Phi_p = n_{int} \exp \left(\frac{qV_p}{k_B T} \right). \quad (3.20)$$

3.3 Constant Current van Roosbroeck System

Consider a one-dimensional model of the van Roosbroeck system and solve for n and p if there is a constant current, J_n and J_p , for both electrons and holes, respectively. We assume that we do not know what the potential V is (e.g. linear, exponential, sinusoidal, etc.). The current equation for electrons becomes

$$qD_n \frac{dn}{dx} - q\mu_n n \frac{dV}{dx} = J_n, \quad (3.21)$$

which is a first order linear ordinary differential equation with constant coefficients that can be solved using an integrating factor as shown in Boyce and DiParma [BD77].

Rewriting the equation using Einstein's relation:

$$\frac{dn}{dx} - \frac{q}{k_B T} n \frac{dV}{dx} = \frac{J_n}{k_B T}, \quad (3.22)$$

we can find the integrating factor:

$$\nu_n(x) = \exp \left(- \int \frac{q}{k_B T} \frac{dV}{dx} dx \right). \quad (3.23)$$

Thus, our integrating factor becomes

$$\nu_n(x) = \exp \left(- \frac{q(V(x) - V_n)}{k_B T} \right). \quad (3.24)$$

Our equation, thus, becomes

$$(n(x)\nu_n(x))' = \frac{J_n}{k_B T} \nu_n(x). \quad (3.25)$$

Once we integrate both sides we have and letting $\beta = \frac{q}{k_B T}$

$$n(x) = \exp \left(\beta(V(x) - V_n) \right) \frac{J_n}{k_B T} \int \exp \left(-\beta(V(x) - V_n) \right) dx \quad (3.26)$$

or

$$n(x) = \exp(\beta V(x)) \frac{J_n}{k_B T} \int \exp(-\beta V(x)) dx. \quad (3.27)$$

Similarly,

$$p(x) = \exp \left(-(\beta(V(x) - V_n)) \right) \frac{J_p}{k_B T} \int \exp \left(\beta(V(x) - V_n) \right) dx \quad (3.28)$$

or

$$p(x) = \exp(-\beta V(x)) \frac{J_p}{k_B T} \int \exp(\beta V(x)) dx. \quad (3.29)$$

3.4 Constant Current with Linear Potential van Roosbroeck System

Now assume that along with a constant current J_n we have a linear potential $\frac{dV}{dx} = -E$. If we solve the van Roosbroeck system we will get the following:

$$\frac{dn}{dx} + \frac{qE}{k_B T} n = \frac{J_n}{k_B T}, \quad (3.30)$$

which is a separable differential equation and is solved by the following

$$\frac{dn}{dx} = \frac{1}{k_B T} \left(J_n + qnE \right), \quad (3.31)$$

$$\frac{dn}{J_n + qnE} = \frac{1}{k_B T} dx, \quad (3.32)$$

and solution is:

$$n(x) = \frac{J_n - \exp\left(\frac{1}{k_B T}x\right)}{qE}. \quad (3.33)$$

Similarly for the holes,

$$p(x) = \frac{-J_p + \exp\left(\frac{1}{k_B T}x\right)}{qE}. \quad (3.34)$$

3.5 Gummel Iteration

Now that we have two formulations for the solutions to the two drift-diffusion equations we can use their solutions n and p to solve the Poisson equation. To solve this we will implement Gummel iteration, which solves the coupled set of drift-diffusion equations and Poisson equation using a decoupling procedure. For Gummel iteration we will utilize Slotboom variables instead of the Quasi-Fermi level variables. Given some initial V^0 we use Slotboom variables to solve for

$n^0 = n_{int} \exp\left(\frac{-V^0}{k_B T}\right)$ and $p^0 = n_{int} \exp\left(\frac{qV^0}{k_B T}\right)$. We can then use n^0 and p^0 to solve the Poisson equation for $V^1 = V^0 + \Delta V$.

$$\frac{d^2 V^1}{dx^2} = -\frac{q}{\varepsilon} \left(n_{int} \exp\left(\frac{-qV^1}{k_B T}\right) - n_{int} \exp\left(\frac{qV^1}{k_B T}\right) + C \right) \quad (3.35)$$

By normalizing and letting $C = 0$ we can write the linearized system as

$$\frac{d^2(V^0 + \Delta V)}{dx^2} = -\frac{qn_{int}}{\varepsilon} \left(\exp(-V^0) \exp(-\Delta V) - \exp(V^0) \exp(\Delta V) \right). \quad (3.36)$$

Now we use the linearization of $\exp(\pm \Delta V) = 1 \pm \Delta V$ to write the Poisson equation as

$$\frac{d^2 V^0}{dx^2} + \frac{d^2 \Delta V}{dx^2} = -\frac{qn_{int}}{\varepsilon} \left(\exp(-V^0)(-1 - \Delta V) - \exp(V^0)(1 + \Delta V) \right). \quad (3.37)$$

In order to solve for V^1 , we must now solve for ΔV by solving the discretized tridiagonal system below

$$\frac{V_{i+1}^0 - 2V_i^0 + V_{i-1}^0}{\Delta x^2} + \frac{\Delta V_{i+1} - 2\Delta V_i + \Delta V_{i-1}}{\Delta x^2} = -\frac{qn_{int}}{\varepsilon} \left(\exp(-V^0)(-1 - \Delta V_i) - \exp(V^0)(1 + \Delta V_i) \right). \quad (3.38)$$

Once the linearized Poisson equation is solved for the potential V^1 , it is plugged back into the drift-diffusion equations and solved using Slotboom variables. Then we repeat the procedure by plugging these new Slotboom variables back into the Poisson equation and solve until our solution converges within a set tolerance.

In general, for a V^k we can use Slotboom variables to find n^k and p^k . Then use n^k and p^k to find V^{k+1} , then find n^{k+1} and p^{k+1} and repeat the process [Gum64]. That is, with an initial set of data V^k, n^k , and p^k we want to find $V^{k+1} = V^k + \Delta V$ by plugging our initial data into the Poisson equation then check for convergence. We will use Gummel iteration in order to solve the full van Roosbroeck system in Chapter 5.

3.6 Damping

Another Gummel-related iteration scheme to solve the Poisson equation uses a linear combination of the newly computed potential, V^{k+1} , and current potential, V^k , as well as a damping constant, α . As stated, the scheme follows a Gummel iteration, but once the new potential V^{k+1} is calculated we will use

$$V^{k+1} = \alpha V^{k+1} + (1 - \alpha) V^k \quad (3.39)$$

as the new potential. In fact, the same can be done for the concentrations of electrons and holes.

This method can reduce numerical instabilities and converge to thermal equilibrium quicker. As Brinkman [Bri12] notes, if we consider $\alpha = 1$, then we are simply using the Gummel iteration described previously..

3.7 Drift-Diffusion in van Roosbroeck System

We will now look at the drift-diffusion equations given in the van Roosbroeck system with their physical parameters. The drift-diffusion equation for the concentration of electrons is given by

$$n_t = \frac{\mu_n k_B T}{q} n_{xx} - \mu_n E n_x \quad (3.40)$$

where $E = -\frac{dV}{dx}$.

Using a forward finite difference method

$$\frac{n_i^{j+1} - n_i^j}{\Delta t} = \mu_n V_T \left(\frac{n_{i+1}^{j+1} - 2n_i^{j+1} + n_{i-1}^{j+1}}{\Delta x^2} \right) - \mu_n \left(\frac{-(V_{i+1} - V_i)}{\Delta x} \right) \left(\frac{n_{i+1}^{j+1} - n_i^{j+1}}{\Delta x} \right). \quad (3.41)$$

Letting $\alpha_1 = \frac{\mu_n V_T \Delta t}{\Delta x^2}$, $\alpha_2 = \frac{\mu_n \Delta t}{\Delta x}$, $V_T = \frac{k_B T}{q}$ the thermal voltage, and $dV_i = -\frac{V_{i+1} - V_i}{\Delta x}$ we have the following:

$$n_i^j = n_{i+1}^{j+1}(-\alpha_1 + \alpha_2 dV_i) + n_i^{j+1}(1 + 2\alpha_1 - \alpha_2 dV_i) + n_{i-1}^{j+1}(-\alpha_1) \quad (3.42)$$

Using a backward finite difference method

$$\frac{n_i^{j+1} - n_i^j}{\Delta t} = \mu_n V_T \left(\frac{n_{i+1}^{j+1} - 2n_i^{j+1} + n_{i-1}^{j+1}}{\Delta x^2} \right) - \mu_n \left(\frac{-(V_i - V_{i-1})}{\Delta x} \right) \left(\frac{n_i^{j+1} - n_{i-1}^{j+1}}{\Delta x} \right). \quad (3.43)$$

$$n_i^j = n_{i+1}^{j+1}(-\alpha_1) + n_i^{j+1}(1 + 2\alpha_1 + \alpha_2 dV_i) + n_{i-1}^{j+1}(-\alpha_1 - \alpha_2 dV_i) \quad (3.44)$$

Similarly, the drift-diffusion equation for the concentration of holes we can use a forward finite difference method

$$\frac{p_i^{j+1} - p_i^j}{\Delta t} = \mu_p V_T \left(\frac{p_{i+1}^{j+1} - 2p_i^{j+1} + p_{i-1}^{j+1}}{\Delta x^2} \right) + \mu_p \left(\frac{-(V_{i+1} - V_i)}{\Delta x} \right) \left(\frac{p_{i+1}^{j+1} - p_i^{j+1}}{\Delta x} \right). \quad (3.45)$$

Letting $\beta_1 = \frac{\mu_p V_T \Delta t}{\Delta x^2}$, $\beta_2 = \frac{\mu_p \Delta t}{\Delta x}$, and $dV_i = -\frac{V_{i+1} - V_i}{\Delta x}$ we have the following:

$$p_i^j = p_{i+1}^{j+1}(-\beta_1 - \beta_2 dV_i) + p_i^{j+1}(1 + 2\beta_1 + \beta_2 dV_i) + p_{i-1}^{j+1}(-\beta_1). \quad (3.46)$$

Using a backward finite difference method

$$\frac{p_i^{j+1} - p_i^j}{\Delta t} = \mu_p V_T \left(\frac{p_{i+1}^{j+1} - 2p_i^{j+1} + p_{i-1}^{j+1}}{\Delta x^2} \right) + \mu_p \left(\frac{-(V_i - V_{i-1})}{\Delta x} \right) \left(\frac{p_i^{j+1} - p_{i-1}^{j+1}}{\Delta x} \right). \quad (3.47)$$

$$p_i^j = p_{i+1}^{j+1}(-\beta_1) + p_i^{j+1}(1 + 2\beta_1 - \beta_2 dV_i) + p_{i-1}^{j+1}(-\beta_1 + \beta_2 dV_i). \quad (3.48)$$

If we compare these difference equations with those of Section 1.1, we can see that these equations are more complex because of the varying potentials. When programming we would like to avoid this. In order to do so, we will discretize the current and continuity equations using the Scharfetter-Gummel finite difference scheme introduced in the next chapter.

CHAPTER 4

SCHARFETTER-GUMMEL SCHEME

4.1 Scharfetter-Gummel Discretization

Mathematically, the challenge in solving the van Roosbroeck system lies in the nonlinearities, the boundary conditions, and the necessity to accurately describe the physical properties of a semiconductor device. The finite difference scheme created by Scharfetter and Gummel [SG69] in 1969 is used to handle these nonlinearities in order to model and simulate semiconductor devices as accurately as possible. In the following sections, we will derive the full Scharfetter-Gummel discretization for the continuity and current equations of the van Roosbroeck system. We will then solve the fully discretized van Roosbroeck system with the Poisson equation and appropriate boundary conditions.

4.1.1 Current and Continuity Equations

We first look at the current equations of electrons and holes. We can approximate the electron (or hole) current at the midpoint of the intervals $\Omega_{i+1} = [x_i, x_{i+1}]$ for $i = 0, 1, 2, \dots, N$ by the using the electron current equation:

$$J_n = q\mu_n n(x) \left(-\frac{dV}{dx} \right) + qD_n \left(\frac{dn}{dx} \right). \quad (4.1)$$

To simplify the notation, we will drop the subscript n denoting electrons and reintroduce them as superscripts as to not confuse them with the subscripts, which are used for the gridpoints. We will also use Δx instead of dx because we are using a finite difference scheme.

$$J_{i+\frac{1}{2}}^n = q\mu_n n(x) \left(-\frac{\Delta V}{\Delta x} \right) + qD_n \left(\frac{\Delta n}{\Delta x} \right) \quad (4.2)$$

The above equation is a first order linear ordinary differential equation that we can solve by using an integrating factor σ defined as:

$$\sigma(x) = \exp \left(\int \frac{1}{V_T} \left(-\frac{\Delta V}{\Delta x} \right) dx \right) = \exp \left(-\frac{1}{V_T} \frac{\Delta V}{\Delta x} x \right) \quad (4.3)$$

Multiplying the current equation and integrating over the interval Ω_{i+1} we obtain:

$$\int_{\Omega_{i+1}} \frac{J_{i+\frac{1}{2}}}{qD} \sigma(x) dx = \int_{\Omega_{i+1}} \frac{d}{dx} \left[\sigma(x) n(x) \right] dx \quad (4.4)$$

After integrating we have:

$$-\frac{J_{i+\frac{1}{2}}}{qD} \frac{V_T}{\frac{\Delta V}{\Delta x}} [\sigma(x_{i+1}) - \sigma(x_i)] = \sigma(x_{i+1}) n_{i+1} - \sigma(x_i) n_i \quad (4.5)$$

and solving for $J_{i+\frac{1}{2}}$:

$$J_{i+\frac{1}{2}} = -\frac{qD}{V_T} \frac{\Delta V}{\Delta x} \left[\frac{\sigma(x_{i+1}) n_{i+1} - \sigma(x_i) n_i}{\sigma(x_{i+1}) - \sigma(x_i)} \right] \quad (4.6)$$

After some algebraic manipulation and letting $\Delta V = V_{i+1} - V_i$ we obtain:

$$J_{i+\frac{1}{2}}^n = \frac{q\mu_n V_T}{\Delta x} \left[\mathcal{B} \left(\frac{V_{i+1} - V_i}{V_T} \right) n_{i+1} - \mathcal{B} \left(\frac{V_i - V_{i+1}}{V_T} \right) n_i \right], \quad (4.7)$$

where $\mathcal{B}(x) = \frac{x}{\exp(x)-1}$ is the Bernoulli function. And for the interval Ω_{i-1} , we can easily see that we have:

$$J_{i-\frac{1}{2}}^n = \frac{q\mu_n V_T}{\Delta x} \left[\mathcal{B} \left(\frac{V_i - V_{i-1}}{V_T} \right) n_i - \mathcal{B} \left(\frac{V_{i-1} - V_i}{V_T} \right) n_{i-1} \right] \quad (4.8)$$

Analogously, for the holes we have:

$$J_{i+\frac{1}{2}}^p = -\frac{q\mu_p V_T}{\Delta x} \left[\mathcal{B}\left(\frac{V_i - V_{i+1}}{V_T}\right) p_{i+1} - \mathcal{B}\left(\frac{V_{i+1} - V_i}{V_T}\right) p_i \right] \quad (4.9)$$

and

$$J_{i-\frac{1}{2}}^p = -\frac{q\mu_p V_T}{\Delta x} \left[\mathcal{B}\left(\frac{V_{i-1} - V_i}{V_T}\right) p_i - \mathcal{B}\left(\frac{V_i - V_{i-1}}{V_T}\right) p_{i-1} \right]. \quad (4.10)$$

These above 4 equations are the Scharfetter-Gummel discretization of the current equations for electrons and holes. We will now use these discretizations of the current equations to discretize the continuity equations implicitly as:

$$\frac{n_{i,j+1} - n_{i,j}}{\Delta t} = \frac{J_{i+\frac{1}{2},j+1}^n - J_{i-\frac{1}{2},j+1}^n}{q\Delta x} + R_{i,j+1} \quad (4.11)$$

and

$$\frac{p_{i,j+1} - p_{i,j}}{\Delta t} = -\frac{J_{i+\frac{1}{2},j+1}^p - J_{i-\frac{1}{2},j+1}^p}{q\Delta x} + R_{i,j+1}. \quad (4.12)$$

In order to solve the above difference equations for n and p , Selberherr [Sel84] says to create a tridiagonal system and assume that the recombination term $R = 0$. Our system becomes:

$$n_{i,j} = n_{i,j+1} - \frac{\mu_n V_T \Delta t}{\Delta x^2} \left[\mathcal{B}_{(i+1,i)} n_{i+1,j+1} - (\mathcal{B}_{(i,i+1)} + \mathcal{B}_{(i,i-1)}) n_{i,j+1} + \mathcal{B}_{(i-1,i)} n_{i-1,j+1} \right] \quad (4.13)$$

where $\mathcal{B}_{(n,m)} = \mathcal{B}\left(\frac{V_n - V_m}{V_T}\right)$ represents the flux across the grid points n and m .

For now, we will assume no specific boundary conditions, but will implement them later. The discretization above leads to a tridiagonal system for the concentrations of electrons and holes given by

$$\vec{n}_j = (I + N) \vec{n}_{j+1} \quad (4.14)$$

where

$$N = \frac{\mu_n V_T \Delta t}{\Delta x^2} \begin{bmatrix} \mathcal{B}_{(1,2)} + \mathcal{B}_{(1,0)} & -\mathcal{B}_{(2,1)} & 0 & \dots & \dots & 0 & 0 \\ -\mathcal{B}_{(1,2)} & \mathcal{B}_{(2,3)} + \mathcal{B}_{(2,1)} & -\mathcal{B}_{(3,2)} & 0 & \dots & \dots & 0 \\ 0 & -\mathcal{B}_{(2,3)} & \mathcal{B}_{(3,4)} + \mathcal{B}_{(3,2)} & -\mathcal{B}_{(4,3)} & \ddots & \ddots & \vdots \\ \vdots & \ddots & -\mathcal{B}_{(3,4)} & \ddots & \ddots & \ddots & \vdots \\ \vdots & & \ddots & \ddots & \ddots & \ddots & 0 \\ 0 & & \ddots & \ddots & \ddots & \ddots & -\mathcal{B}_{(n,n-1)} \\ 0 & 0 & \dots & \dots & 0 & -\mathcal{B}_{(n-1,n)} & \mathcal{B}_{(n,n+1)} + \mathcal{B}_{(n,n-1)} \end{bmatrix} \quad (4.15)$$

Analogously, for p we have

$$p_{i,j} = p_{i,j+1} - \frac{\mu_p V_T \Delta t}{\Delta x^2} \left[\mathcal{B}_{(i,i+1)} p_{i+1,j+1} - (\mathcal{B}_{(i+1,i)} + \mathcal{B}_{(i-1,i)}) p_{i,j+1} + \mathcal{B}_{(i,i-1)} p_{i-1,j+1} \right] \quad (4.16)$$

and

$$\vec{p}_j = (I + P) \vec{p}_{j+1} \quad (4.17)$$

where

$$P = \frac{\mu_p V_T \Delta t}{\Delta x^2} \begin{bmatrix} \mathcal{B}_{(2,1)} + \mathcal{B}_{(0,1)} & -\mathcal{B}_{(1,2)} & 0 & \dots & \dots & 0 & 0 \\ -\mathcal{B}_{(2,1)} & \mathcal{B}_{(3,2)} + \mathcal{B}_{(1,2)} & -\mathcal{B}_{(2,3)} & 0 & \dots & \dots & 0 \\ 0 & -\mathcal{B}_{(3,2)} & \mathcal{B}_{(4,3)} + \mathcal{B}_{(2,3)} & -\mathcal{B}_{(3,4)} & \ddots & \ddots & \vdots \\ \vdots & \ddots & -\mathcal{B}_{(4,3)} & \ddots & \ddots & \ddots & \vdots \\ \vdots & & \ddots & \ddots & \ddots & \ddots & 0 \\ 0 & & \ddots & \ddots & \ddots & \ddots & -\mathcal{B}_{(n-1,n)} \\ 0 & 0 & \dots & \dots & 0 & -\mathcal{B}_{(n,n-1)} & \mathcal{B}_{(n+1,n)} + \mathcal{B}_{(n-1,n)} \end{bmatrix} \quad (4.18)$$

4.1.2 The Poisson Equation

Finally, we need to discretize the Poisson equation as we did when discussing Gummel iteration

$$-\frac{\epsilon}{\Delta x^2} [V_{i+1,j+1} - 2V_{i,j+1} + V_{i-1,j+1}] = q(p_{i,j} - n_{i,j} + C_{i,j}). \quad (4.19)$$

Looking at the system we have the following:

$$P_M \vec{V}_{j+1} - B\vec{C}V_{j+1} = \frac{q\Delta x^2}{\epsilon} (\vec{p}_j - \vec{n}_j + \vec{C}_j) \quad (4.20)$$

where

$$P_M = \begin{bmatrix} 2 & -1 & 0 & \dots & \dots & 0 & 0 \\ -1 & 2 & -1 & 0 & \dots & \dots & \vdots \\ 0 & -1 & 2 & -1 & \ddots & & \\ \vdots & \ddots & -1 & \ddots & \ddots & \ddots & \vdots \\ & & & \ddots & \ddots & \ddots & 0 \\ \vdots & & & & \ddots & \ddots & -1 \\ 0 & 0 & \dots & \dots & 0 & -1 & 2 \end{bmatrix} \quad (4.21)$$

and

$$B\vec{C}V_{j+1} = \begin{bmatrix} V_{0,j+1} \\ 0 \\ \vdots \\ \vdots \\ 0 \\ V_{N+1,j+1} \end{bmatrix}. \quad (4.22)$$

Now we can use a Gummel iteration to solve our Poisson equation alongside the Scharfetter-Gummel finite difference scheme. For now, we have not assumed any

boundary conditions for V , but in the next section we will impose more realistic boundary conditions.

4.2 Boundary Conditions

Previously, we assumed periodic boundary conditions for the concentration of electrons and holes, but for more realistic modeling and simulation we use Ohmic contacts, which, once implemented, amount to finding Dirichlet boundary conditions. Unfortunately, implementing the boundary conditions for a system of partial differential equations is much more difficult than discretizing the system itself. As Selberherr [Sel84] points out, we have to find three sets of boundary conditions corresponding to each equation in the van Roosbroeck system: one for the electrons, holes, and potential. To find the boundary conditions for the electrons and holes, we assume thermal equilibrium:

$$np - n_{int}^2 = 0 \quad (4.23)$$

$$n - p - C = 0. \quad (4.24)$$

These two equations can be solved to yield Dirichlet boundary conditions for the concentration of electrons and holes:

$$n = \frac{\sqrt{C^2 + 4n_{int}^2} + C}{2} \quad (4.25)$$

$$p = \frac{\sqrt{C^2 + 4n_{int}^2} - C}{2}. \quad (4.26)$$

The Dirichlet boundary conditions can be discretized as:

$$n_{i,j} = \frac{\sqrt{C_{i,j}^2 + 4n_{int}^2} + C_{i,j}}{2} \quad (4.27)$$

and

$$p_{i,j} = \frac{\sqrt{C_{i,j}^2 + 4n_{int}^2} - C_{i,j}}{2}. \quad (4.28)$$

Looking at the Scharfetter-Gummel discretization of the continuity equation for electrons, we can now implement the Dirichlet boundary conditions given by

$$n_{0,j} = \frac{\sqrt{C_{0,j}^2 + 4n_{int}^2} + C_{0,j}}{2} \quad (4.29)$$

$$n_{N+1,j} = \frac{\sqrt{C_{N+1,j}^2 + 4n_{int}^2} + C_{N+1,j}}{2}. \quad (4.30)$$

For our first grid point $i = 1$ and last grid point $i = N$ we have:

$$n_{1,j} = n_{1,j+1} - \frac{\mu_n V_T \Delta t}{\Delta x^2} \left[\mathcal{B}_{(2,1)} n_{2,j+1} - (\mathcal{B}_{(1,2)} + \mathcal{B}_{(1,0)}) n_{1,j+1} + \mathcal{B}_{(0,1)} n_{0,j+1} \right] \quad (4.31)$$

$$n_{N,j} = n_{N,j+1} - \frac{\mu_n V_T \Delta t}{\Delta x^2} \left[\mathcal{B}_{(N+1,N)} n_{N+1,j+1} - (\mathcal{B}_{(N,N+1)} + \mathcal{B}_{(N,N-1)}) n_{N,j+1} + \mathcal{B}_{(N-1,N)} n_{N-1,j+1} \right] \quad (4.32)$$

In these discretizations, we can use the substitution to include the boundary conditions defined previously. It is easy to see that we can now write a system of the form (still assuming $R = 0$):

$$(I + N) \vec{n}_{j+1} + B \vec{C} n_{j+1} = \vec{n}_j \quad (4.33)$$

where

$$B\vec{C}n_{j+1} = -\frac{\mu_n V_T \Delta t}{\Delta x^2} \begin{bmatrix} \mathcal{B}_{(0,1)} n_{0,j+1} \\ 0 \\ \vdots \\ \vdots \\ 0 \\ \mathcal{B}_{(N+1,N)} n_{N+1,j+1} \end{bmatrix}. \quad (4.34)$$

Similarly, for holes we obtain the following system:

$$(I + N)\vec{p}_{j+1} + B\vec{C}p_{j+1} = \vec{p}_j \quad (4.35)$$

where

$$B\vec{C}p_{j+1} = -\frac{\mu_p V_T \Delta t}{\Delta x^2} \begin{bmatrix} \mathcal{B}_{(1,0)} p_{0,j+1} \\ 0 \\ \vdots \\ \vdots \\ 0 \\ \mathcal{B}_{(N,N+1)} p_{N+1,j+1} \end{bmatrix}. \quad (4.36)$$

Now to find the boundary conditions for the potential. Again, we assume thermal equilibrium and solve the Poisson equation for a homogeneously doped semiconductor with no external forces ($V = 0$). This amounts to solving for the built-in potential denoted by V_{bi} . We use the Quasi-Fermi formulation

$$n = n_{int} \exp \left(\frac{V_{bi}}{V_T} \right) \quad (4.37)$$

$$p = n_{int} \exp \left(-\frac{V_{bi}}{V_T} \right) \quad (4.38)$$

to solve for V_{bi} . The calculation is as follows

$$0 = n_{int} \exp \left(\frac{V_{bi}}{V_T} \right) - n_{int} \exp \left(-\frac{V_{bi}}{V_T} \right) - C \quad (4.39)$$

$$0 = \left[\exp \left(\frac{V_{bi}}{V_T} \right) \right]^2 - \frac{C}{n_{int}} \exp \left(\frac{V_{bi}}{V_T} \right) - n_{int}. \quad (4.40)$$

The quadratic equation can be solved to yield

$$V_{bi} = V_T \ln \left[\frac{C + \sqrt{C^2 + 4n_{int}^2}}{2n_{int}} \right]. \quad (4.41)$$

We will use the built-in potential as our Dirichlet boundary conditions for the potential. Thus,

$$V_{0,j+1} = V_{N+1,j+1} = V_{bi}. \quad (4.42)$$

4.3 Slotboom Discretization

The Scharfetter-Gummel finite difference scheme discretized the current equations and yielded a flux function which we denoted as $\mathcal{B} = \frac{x}{\exp(x)-1}$. This paper is concerned with the solutions to the van Roosbroeck system using a different flux function, which will be derived in this section. Using an integrating factor, the current equation

$$J_n = q\mu_n n E + qD_n \left(\frac{dn}{dx} \right) \quad (4.43)$$

can be rewritten as

$$J_n = qD_n \exp\left(-\frac{E}{V_T}\right) \frac{d}{dx} \left[\exp\left(\frac{E}{V_T}\right) n \right]. \quad (4.44)$$

As in the Scharfetter-Gummel discretization, we can discretize the equation above at the midpoint of the intervals $\Omega_{i+1} = [x_i, x_{i+1}]$ and remember that $E = -\frac{dV}{dx}$. However, a problem arises when we try to discretize E which appears outside the differentiation. We can either discretize at x_i using V_i or x_{i+1} using V_{i+1} . In order to deal with this, we will use an average given by $\frac{V_{i+1} + V_i}{2}$. Using an average of the potential will give

$$J_{i+\frac{1}{2}} = \frac{q\mu_n V_T}{\Delta x} \exp\left(-\frac{V_{i+1} + V_i}{2V_T}\right) \left[\exp\left(\frac{V_{i+1}}{V_T}\right) n_{i+1} - \exp\left(\frac{V_i}{V_T}\right) n_i \right] \quad (4.45)$$

which leads to

$$J_{i+\frac{1}{2}} = \frac{q\mu_n V_T}{\Delta x} \left[\exp\left(\frac{V_{i+1} - V_i}{2V_T}\right) n_{i+1} - \exp\left(\frac{V_i - V_{i+1}}{2V_T}\right) n_i \right]. \quad (4.46)$$

The equation above looks identical to the Scharfetter-Gummel discretization, but instead of using what we will call the Scharfetter-Gummel flux function $(\mathcal{B}_{SG}(x) = \frac{x}{\exp(x)-1})$ we have the Slotboom flux function $(\mathcal{B}_{SB}(x) = \exp(-\frac{x}{2}))$. Figure 4.1 compares the two flux functions.

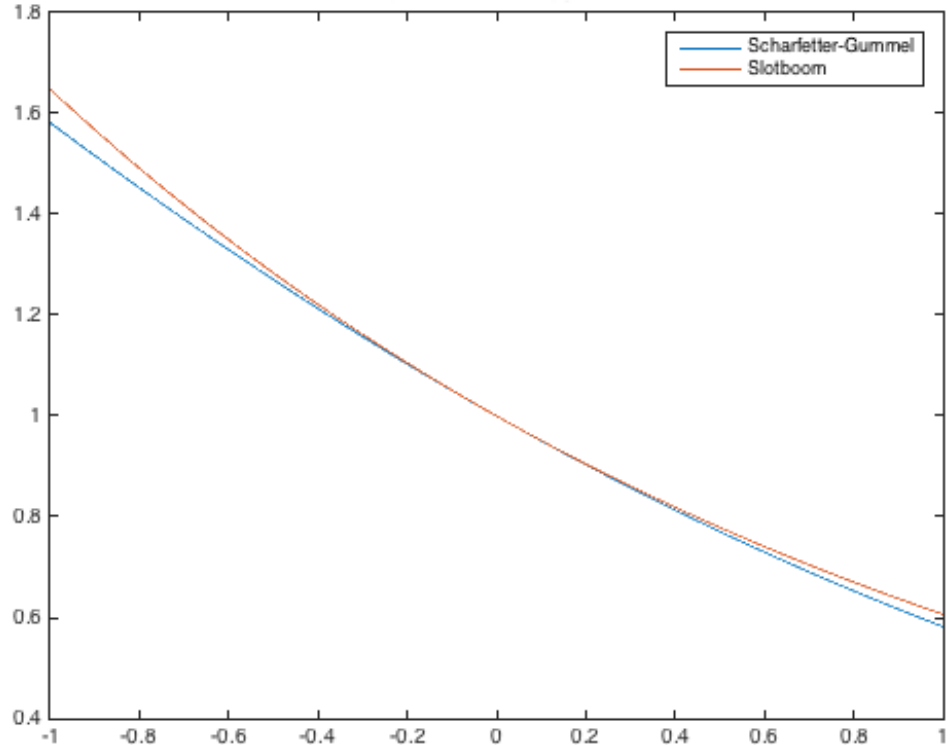


Figure 4.1: Plots of Slotboom and Scharfetter-Gummel flux functions .

We can observe that the two functions start to deviate from each other as $x \rightarrow \pm\infty$. We can also show that the Taylor approximation of $\mathcal{B}_{SB}(x) \approx 1 - \frac{x}{2} + \frac{x^2}{8} - \frac{x^3}{18}$ and $\mathcal{B}_{SG}(x) \approx 1 - \frac{x}{2} + \frac{x^2}{12} - \frac{x^4}{720}$ have the same first order approximation. Ultimately, we will compare the Scharfetter-Gummel flux to the Slotboom flux and note the differences in solutions to the van Roosbroeck system.

CHAPTER 5

SEMICONDUCTOR SIMULATIONS

In this chapter, we will introduce some of the physical parameters of the semiconductors necessary to have meaningful and realistic simulations. We will then present the results of the simulations and interpret them.

5.1 Generation and Recombination

Up until now, we have assumed that there are no recombination or generation, so $R = 0$. We shall now introduce R into our finite difference scheme. Colinge and Colinge [CC06] describe that semiconductors have a crystalline structure and have electrons occupying the valence band and no electrons occupying the conduction band. However, electrons can "jump" from the valence band into "vacancies" in the conduction band at high temperatures. This process is called the generation of an electron-hole pair, i.e. an electron is generated in the conduction band and a hole in the valence band. The inverse process, that is, the transfer of an electron in the conduction band into the lower energy valence band, is called recombination of an electron-hole pair. Generation requires energy and recombination releases energy. During thermal equilibrium, the numbers of generations and recombinations are equal; therefore equilibrium concentrations of electrons and holes are constant over time. Once an external voltage is applied, one can change the concentration of electrons and holes. This applied external bias disturbs thermal equilibrium and causes the concentrations of electrons and holes to stray away from their equilibrium concentrations. The generation and recombination processes attempt to

restore these equilibrium concentrations. Markowich, Ringhofer, and Schmeiser [MRS90] state that the most basic and standard generation-recombination process is described by the Shockley-Read-Hall model.

5.2 Shockley-Read-Hall Model

For the Shockley-Read-Hall generation-recombination term, we have

$$R = \frac{n_{int}^2 - np}{\tau_p(n + n_1) + \tau_n(p + p_1)} \quad (5.1)$$

where τ_n , τ_p , n_1 and p_1 are all material-dependent parameters. In particular, τ_n and τ_p are the electron and hole lifetimes, respectively. For our simulations, we will assume that $n_1 = p_1 = n_{int}$.

In order to implement this in our finite difference scheme, we discretize using a nonlinear partially implicit scheme

$$R_{i,j+1} = \frac{n_{int}^2 - n_{i,j+1}p_{i,j}}{\tau_p(n_{i,j} + n_1) + \tau_n(p_{i,j} + p_1)}. \quad (5.2)$$

Now if we look at our continuity equations with our generation-recombination term, we have the following:

$$\frac{n_{i,j+1} - n_{i,j}}{\Delta t} = \frac{J_{i+\frac{1}{2},j+1}^n - J_{i-\frac{1}{2},j+1}^n}{q\Delta x} + \frac{n_{int}^2 - n_{i,j+1}p_{i,j}}{\tau_p(n_{i,j} + n_1) + \tau_n(p_{i,j} + p_1)} \quad (5.3)$$

which can be put into a tridiagonal system as

$$\begin{aligned} n_{i,j} &= n_{i,j+1} \left[1 + \frac{p_{i,j}\Delta t}{\tau_p(n_{i,j} + n_1) + \tau_n(p_{i,j} + p_1)} \right] - \frac{\mu_n V_T \Delta t}{\Delta x^2} \left[\mathcal{B}_{(i+1,i)} n_{i+1,j+1} - \right. \\ &\quad \left. (\mathcal{B}_{(i,i+1)} + \mathcal{B}_{(i,i-1)}) n_{i,j+1} + \mathcal{B}_{(i-1,i)} n_{i-1,j+1} \right] - \frac{n_{int}^2 \Delta t}{\tau_p(n_{i,j} + n_1) + \tau_n(p_{i,j} + p_1)}. \end{aligned} \quad (5.4)$$

So we have our system

$$\vec{n}_j = \left((1 + \vec{c}_p)I + N \right) \vec{n}_{j+1} + B\vec{C}n_{j+1} + \vec{c}_{int} \quad (5.5)$$

where $\vec{c}_{int} = -\frac{n_{int}^2 \Delta t}{\tau_p(n_{i,j} + n_1) + \tau_n(p_{i,j} + p_1)}$ and $\vec{c}_p = \frac{p_{i,j} \Delta t}{\tau_p(n_{i,j} + n_1) + \tau_n(p_{i,j} + p_1)}$.

Similarly for holes,

$$\begin{aligned} p_{i,j} = p_{i,j+1} & \left[1 + \frac{n_{i,j} \Delta t}{\tau_p(n_{i,j} + n_1) + \tau_n(p_{i,j} + p_1)} \right] - \frac{\mu_p V_T \Delta t}{\Delta x^2} \left[\mathcal{B}_{(i,i+1)} p_{i+1,j+1} - \right. \\ & \left. \left(\mathcal{B}_{(i+1,i)} + \mathcal{B}_{(i-1,i)} \right) p_{i,j+1} + \mathcal{B}_{(i,i-1)} p_{i-1,j+1} \right] - \frac{n_{int}^2 \Delta t}{\tau_p(n_{i,j} + n_1) + \tau_n(p_{i,j} + p_1)}. \end{aligned} \quad (5.6)$$

and

$$\vec{p}_j = \left((1 + \vec{c}_n)I + P \right) \vec{p}_{j+1} + B\vec{C}p_{j+1} + \vec{c}_{int} \quad (5.7)$$

where \vec{c}_{int} is defined as before and $\vec{c}_n = \frac{n_{i,j} \Delta t}{\tau_p(n_{i,j} + n_1) + \tau_n(p_{i,j} + p_1)}$. The matrices P and N are the same as defined previously.

5.3 Doping

We now turn to another term that we have, up until now, ignored in the Poisson equation, the doping concentration C . Before implementing the doping concentration in our simulation, we discuss what doping is. According to Colinge and Colinge [CC06], in most semiconductors, the silicon used is of the highest purity (99.999999%). However, impurities can be injected into the silicon that can change the properties of the semiconductor by increasing electron and hole concentrations. The most common elements that are used are boron, phosphorus, and arsenic. In the crystalline structure itself, the addition of these (dopant) atoms either adds

electrons or subtracts electrons (adds holes). For example, arsenic atoms are called donor atoms because they "donate" an extra electron to the crystal. Boron atoms are called acceptor atoms because they "accept" electrons because they are adding holes to the crystal. Inserting these extra electrons and holes into the crystal contributes to electrical conduction. Another name for these donor and acceptor atoms is doping impurities or dopants and, therefore, we may dope a semiconductor with these impurities.

5.4 PN Junction

There are two types of semiconductors that we can consider: P-type and N-type. A P-type semiconductor is one with acceptor atoms as it has more positive charge (more holes). A N-type semiconductor is one with donor atoms as it has more negative charge (more electrons). When we dope half of our silicon semiconductor with donor atoms and the other half with acceptor atoms, we have a doped semiconductor. Thus, our semiconductor looks like a P-type and N-type silicon semiconductor are in contact. The region of contact is known as a PN junction.

For our simulations, we will consider a doped semiconductor at thermal equilibrium with no external voltage ($V_{ext} = 0$). Once we introduce doping, we add donors to the P-region and add acceptors to the N-region. This corresponds to having two different doping concentrations for each side of the semiconductor: $N_A < 0$ and $N_D > 0$.

5.5 Depletion Region

Colinge and Colinge [CC06] describe that as the semiconductor approaches thermal equilibrium, electrons and holes near the PN junction start to diffuse from

one region to the other. As electrons diffuse from the N-type region to the P-type region, they leave positive donor ions behind in the N-type region. As holes diffuse from the P-type region to the N-type region, they leave negative acceptor ions behind in the P-type region. This creates a small area near the PN junction where there are no charge carriers known as the depletion region. Since there are no charge carriers in the depletion region, it prevents the flow of current. Thus, we have something that acts as an insulator.

5.6 External Voltage and Forward/Reverse Bias

We can take our P-type region and N-type region and hook each side to a battery. To start, we will hook the P-type region up to the positive terminal of the battery and the N-type region to the negative terminal of the battery. Our battery will produce electrons flowing out of the negative terminal into the N-type region. As electrons enter the N-type region, they will repel the electrons to the P-type region and vice versa in the P-type region. This will cause the depletion region of the PN junction to shrink, thereby letting current flow across the semiconductor. This setup of a PN junction is known as forward bias. We can also have the opposite configuration where the P-type region is hooked up to the negative terminal of the battery and the N-type region to the positive terminal of the battery. In this setup, we will see that the electrons in the N-type region will be attracted to the positive terminal of the battery and vice versa in the P-type region. This will cause the depletion region to expand, thereby disallowing current to flow across the semiconductor. Colinge and Colinge [CC06] refer to this setup of a PN junction as reverse bias.

For our simulations, we will be applying an external voltage to the right side

(N-type region) of our PN junction. The sign of V_{ext} will correspond to which bias we are considering. If $V_{ext} < 0$, we will have a forward bias and if $V_{ext} > 0$, we will have a reverse bias. Again, by doping our semiconductor with impurities such as boron or phosphorus, we can change the number of electrons and holes in the semiconductor. This allows electrons to cross into the P-type region from the N-type region.

5.7 Simulation Results

We now illustrate the results of the simulation of a semiconductor. For our simulations, we will simulate using a $10 \mu m$ semiconductor with 100 spatial points and a spatial step of $dx \approx 10^{-7}$. We will run our simulation for a total time of 10^{-8} seconds with 500 time steps and a temporal step of $dt \approx 10^{-11}$. In order to solve the full discretized van Roosbroeck system, we will use Gummel iteration as described in Section 3.5. The programming code is provided in Appendix A.

For the first set of simulations we will have zero doping ($N_A = N_D = 0$), zero initial potential, varying external voltages, and an initial profile of $n_{int} = 1.5 * 10^{16} m^{-3}$ for both electrons and holes. Also, we will use the Slotboom flux function \mathcal{B}_{SB} because for these preliminary results, both \mathcal{B}_{SB} and \mathcal{B}_{SG} agree up to first order. Later we will compute our solutions with the Scharfetter-Gummel flux function \mathcal{B}_{SG} and compare the two. These following plots verify what we expect to see for a semiconductor in thermal equilibrium with these characteristics.

In Figure 5.1, we can see in the case that $V_{ext} < 0$ (forward bias) the electrons will move to the left of the device and for $V_{ext} > 0$ (reverse bias) they will move to the right of the device.

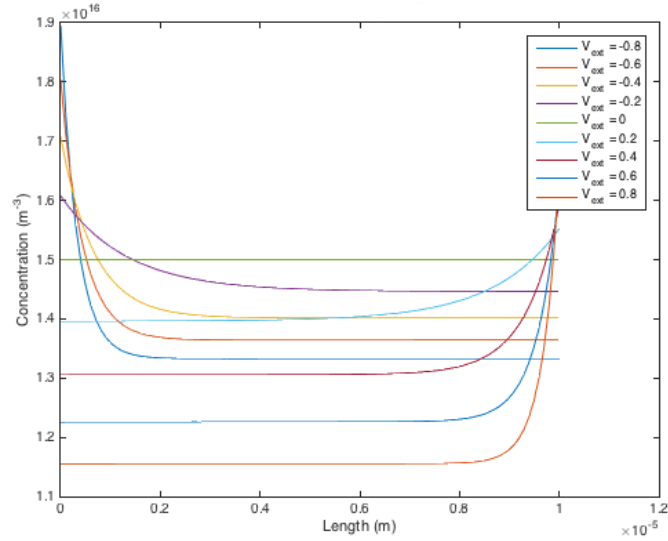


Figure 5.1: Electron concentration of semiconductor at thermal equilibrium with zero doping.

In Figure 5.2, we can see in the case that $V_{ext} < 0$ (forward bias) the holes will move to the right of the device and for $V_{ext} > 0$ (reverse bias) they will move to the left of the device.

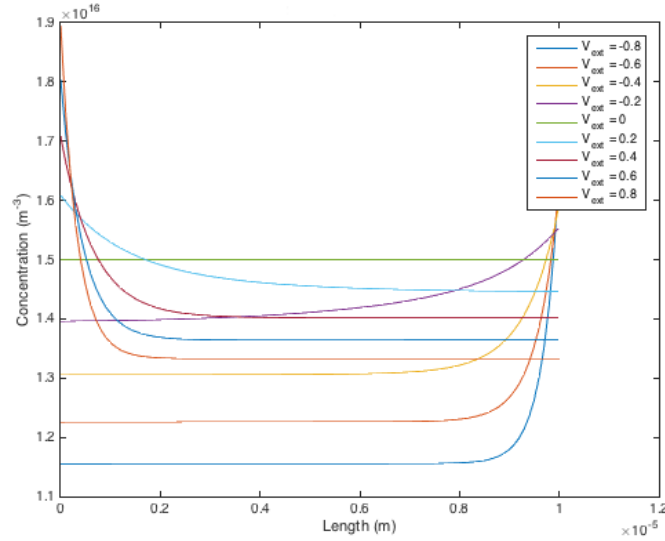


Figure 5.2: Hole concentration of semiconductor at thermal equilibrium.

In both figures, we can see that in the case where $V_{ext} = 0$ that the electron and hole concentrations remain constant at n_{int} throughout the device (no movement).

In Figure 5.3, we can see in the case where $V_{ext} = 0$ the product of the electron and hole concentration is n_{int}^2 as we expect at thermal equilibrium.

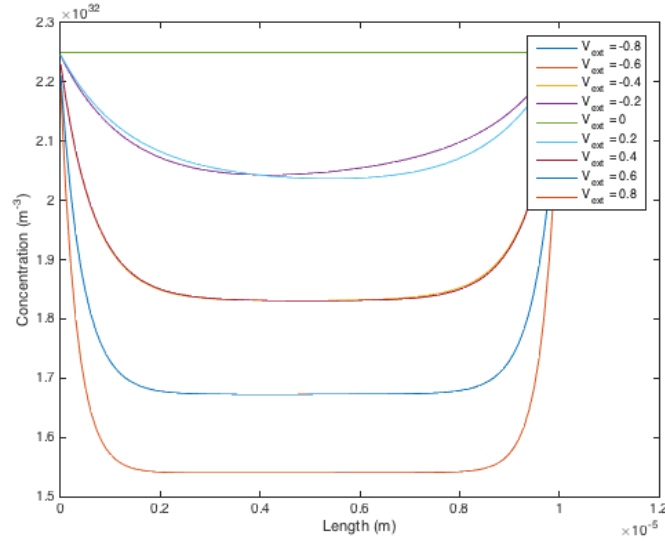


Figure 5.3: Product of electron and hole concentration of semiconductor at thermal equilibrium with zero doping.

In Figure 5.4, we can see in the case where $V_{ext} = 0$ that we have zero potential. Clearly if we apply $V_{ext} > 0$ we will have a positive potential at thermal equilibrium and if we apply $V_{ext} < 0$ we will have a negative potential at thermal equilibrium.

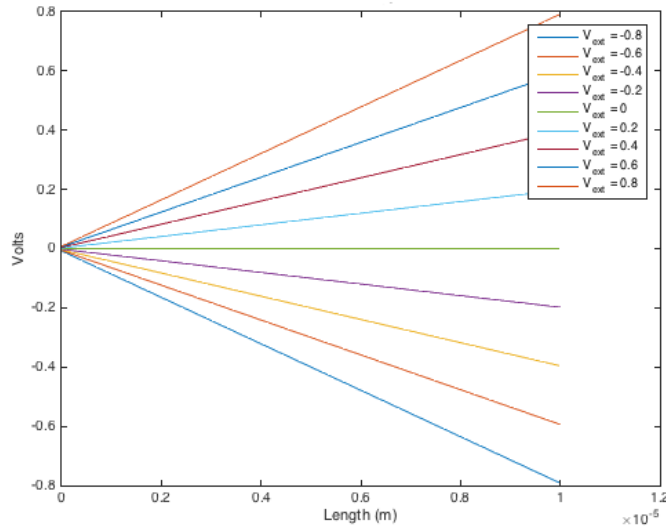


Figure 5.4: Potential of semiconductor at thermal equilibrium with zero doping.

In Figure 5.5, we see the plots of the density, which is the right-hand side of the Poisson equation.

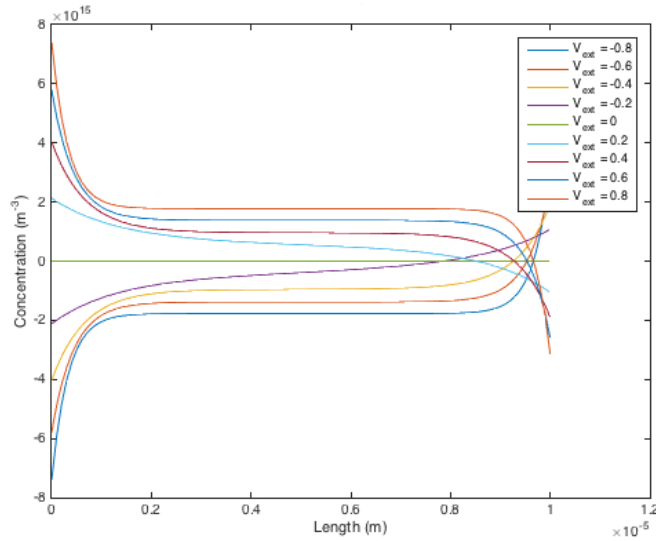


Figure 5.5: The density of semiconductor at thermal equilibrium with zero doping.

In Figure 5.6, we see that the currents for all cases of forward and reverse bias are constant.

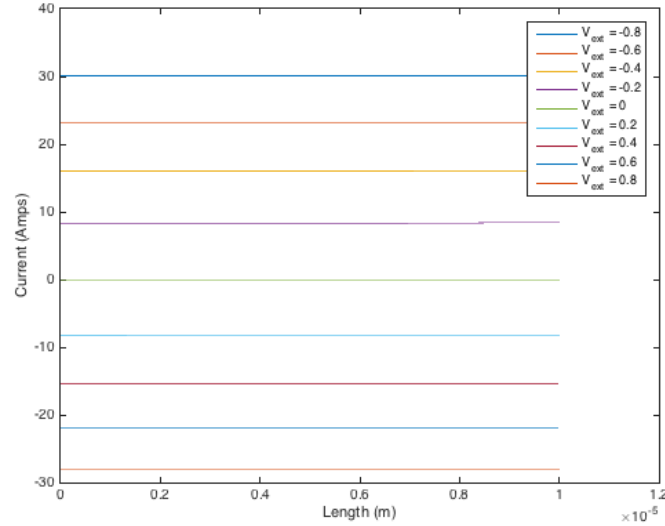


Figure 5.6: The currents of semiconductor at thermal equilibrium with zero doping.

In Figure 5.7, when $V_{ext} = 0$ (no battery hooked up) there should not be any current flowing through the semiconductor, which is confirmed by the simulation.

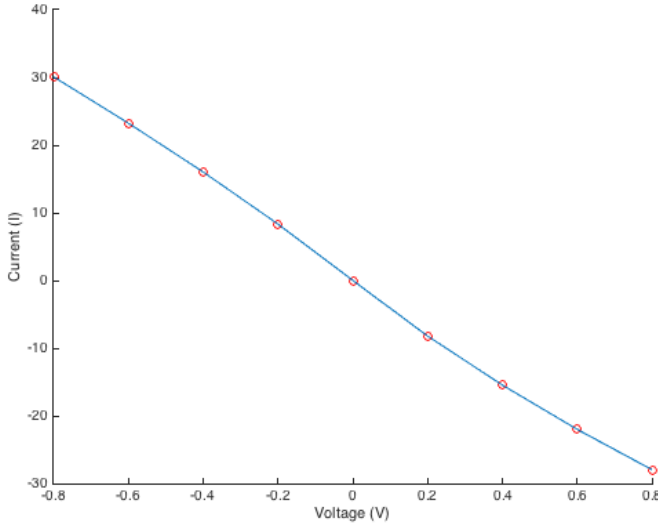


Figure 5.7: The current-voltage plot for different external voltages with zero doping.

5.8 Current-Voltage (IV) Characteristics

As stated before, we are interested in the IV characteristics of doped semiconductors with an external voltage applied. These IV curves will be important when we look at solar cells and their efficiency. We now illustrate the results of a simulation of a semiconductor with an equal amount doping in the P-type and N-type region, zero initial potential, and varying external voltage. Note that since we are adding doping concentrations our initial profile and boundary conditions will change. Our initial profile will follow from the boundary conditions on the concentrations of electrons and holes in Section 4.2. In the P-type region we have $N_A = -10^{18} m^{-3}$ to represent acceptors and in the N-type region we have $N_D = 10^{18} m^{-3}$ to represent donors.

In Figure 5.8, we can see in the case that $V_{ext} < 0$ (forward bias), the depletion region will shrink, which creates a current through the semiconductor. While for

$V_{ext} > 0$ (reverse bias) the electrons will move to the right of the device, thereby increasing the depletion region.

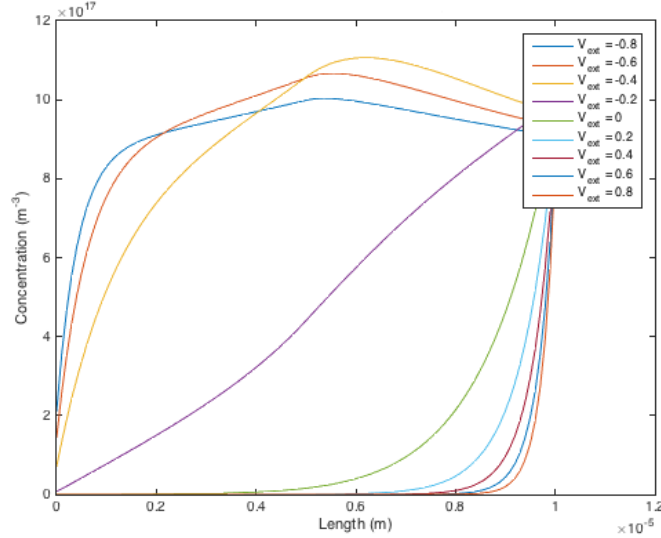


Figure 5.8: Electron concentration of an equally doped semiconductor at thermal equilibrium.

In Figure 5.9, we can see in the case that $V_{ext} < 0$ (forward bias), the depletion region will shrink, which creates a current through the semiconductor. While for $V_{ext} > 0$ (reverse bias) the holes will move to the left of the device, thereby increasing the depletion region.

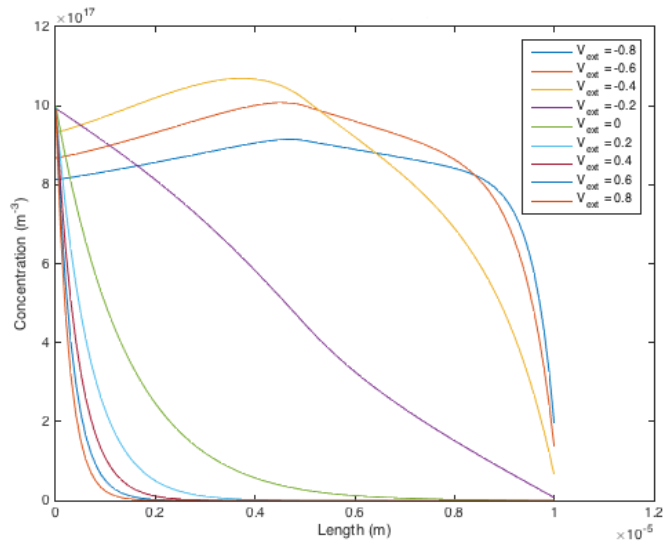


Figure 5.9: Hole concentration of an equally doped semiconductor at thermal equilibrium.

In Figure 5.10, we can see the product of the electron and hole concentration strays away from n_{int}^2 .

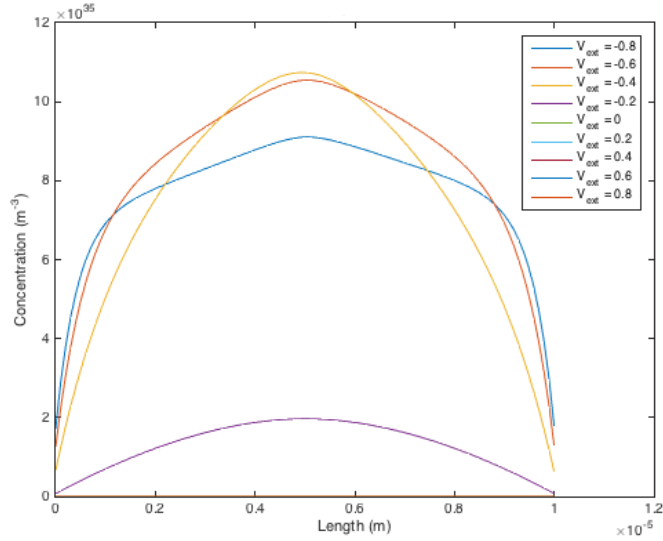


Figure 5.10: Product of electron and hole concentration of an equally doped semiconductor at thermal equilibrium.

In Figure 5.11, one can see that if we apply $V_{ext} > 0$ we will have a positive potential at thermal equilibrium and if we apply $V_{ext} < 0$ we will have a negative potential at thermal equilibrium.

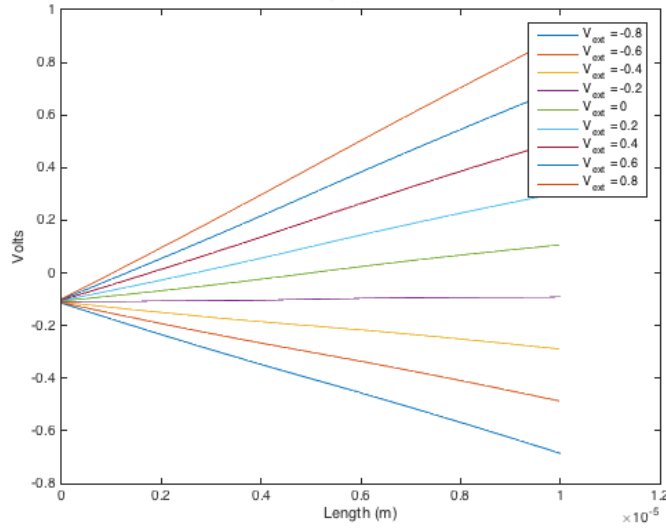


Figure 5.11: Potential of an equally doped semiconductor at thermal equilibrium.

In Figure 5.12, we see the plots of the density, which is the right-hand side of the Poisson equation.

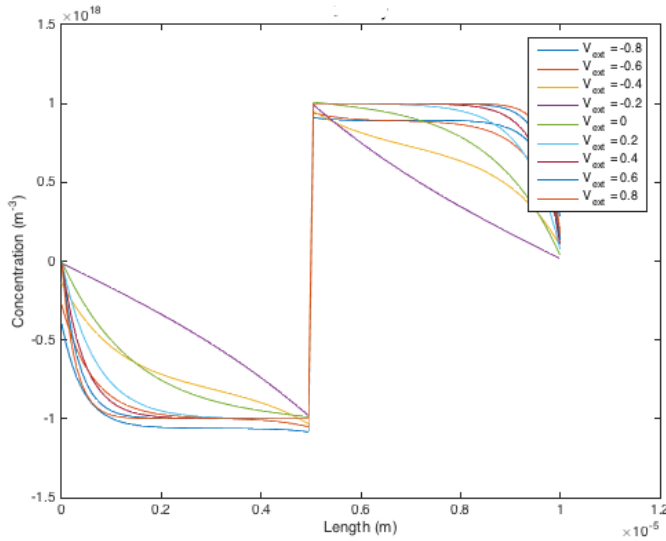


Figure 5.12: The density of an equally doped semiconductor at thermal equilibrium.

In Figure 5.13, when we have $V_{ext} > 0$ (reverse bias) there should not be any current flowing through the semiconductor, which is confirmed by the simulation. When we have $V_{ext} < 0$ (forward bias) there should be current flowing through the semiconductor, which is confirmed by the simulation.

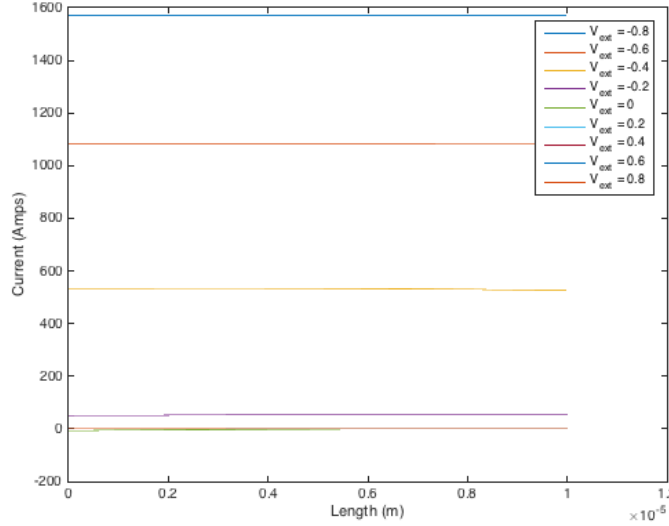


Figure 5.13: The currents of an equally doped semiconductor at thermal equilibrium.

Figure 5.14 verifies the fact that when we have our PN junction in a forward bias setup ($V_{ext} < 0$), there is little to no current. However, when we have our PN junction in a reverse bias set up ($V_{ext} > 0$), there is current running through the device.

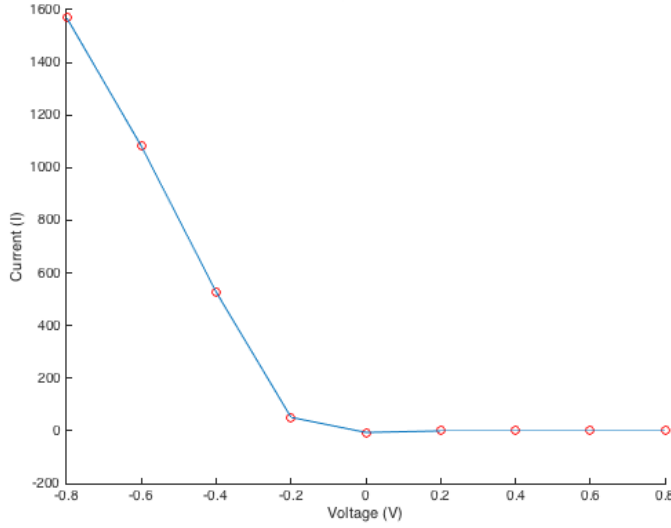


Figure 5.14: The current-voltage plot for different external voltages of equally doped semiconductor at thermal equilibrium.

We now illustrate the results of the simulation of a semiconductor with more doping in the P-type region ($N_A = -10^{18}$, $N_D = 10^{16}$), zero initial potential, and varying external voltage.

In Figure 5.15, we can see in the case that $V_{ext} < 0$ (forward bias), the depletion region will shrink, which creates a current through the semiconductor. While for $V_{ext} > 0$ (reverse bias) the electrons will move to the right of the device, thereby increasing the depletion region.

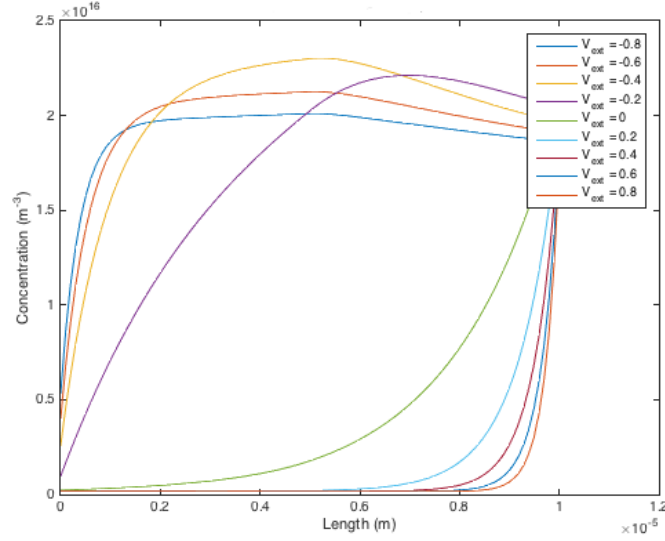


Figure 5.15: Electron concentration of doped semiconductor at thermal equilibrium with higher doping in the P-type region.

In Figure 5.16, we can see in the case that $V_{ext} < 0$ (forward bias), the depletion region will shrink, which creates a current through the semiconductor. While for $V_{ext} > 0$ (reverse bias) the holes will move to the left of the device, thereby increasing the depletion region.

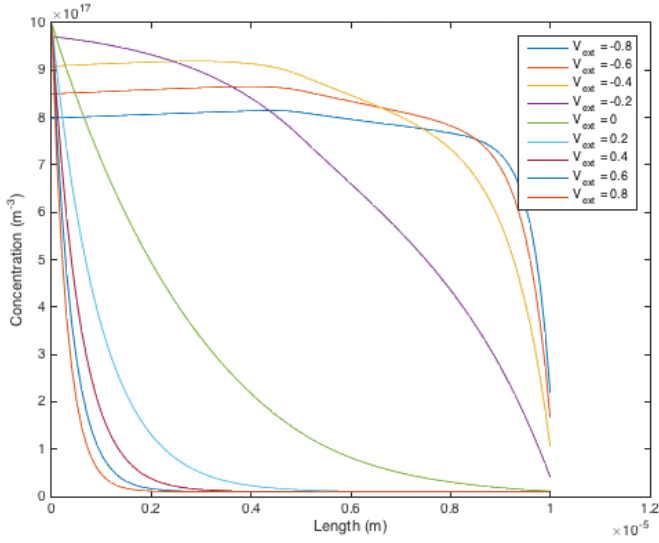


Figure 5.16: Hole concentration of doped semiconductor at thermal equilibrium with higher doping in the P-type region.

In Figure 5.17, we can see the product of the electron and hole concentration strays away from n_{int}^2 .

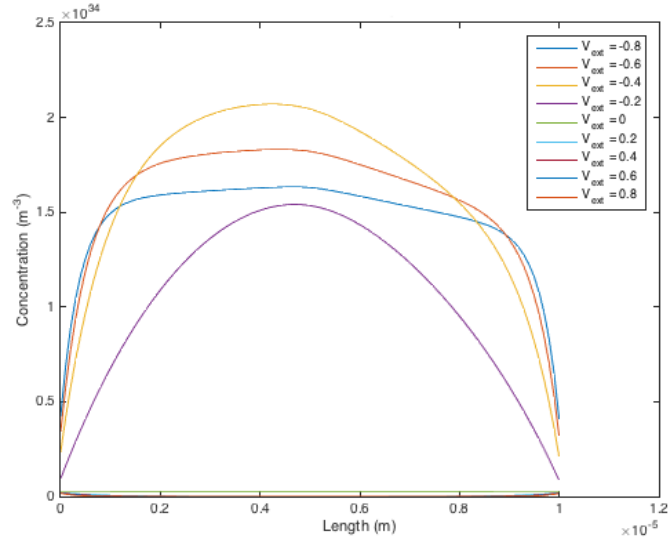


Figure 5.17: Product of electron and hole concentration of doped semiconductor at thermal equilibrium with higher doping in the P-type region.

In Figure 5.18, one can see that if we apply $V_{ext} > 0$ we will have a positive potential at thermal equilibrium and if we apply $V_{ext} < 0$ we will have a negative potential at thermal equilibrium.

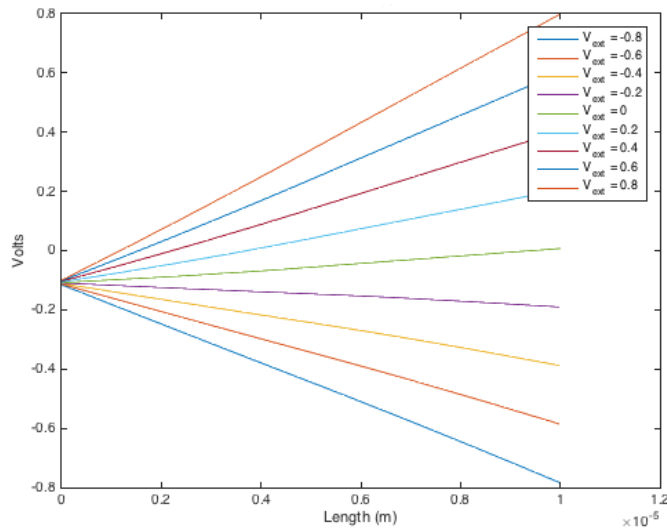


Figure 5.18: Potential of doped semiconductor at thermal equilibrium with higher doping in the P-type region.

In Figure 5.19, we see the plots of the density, which is the right-hand side of the Poisson equation.

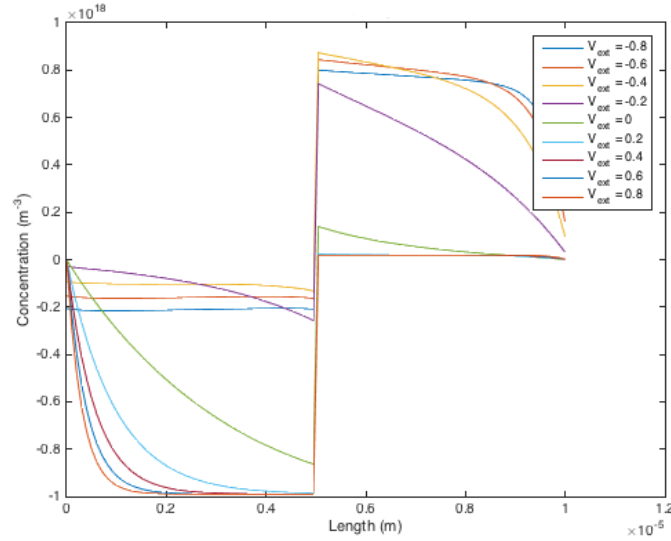


Figure 5.19: The density of doped semiconductor at thermal equilibrium with higher doping in the P-type region.

In Figure 5.20, when we have $V_{ext} > 0$ (reverse bias) there should not be any current flowing through the semiconductor, which is confirmed by the simulation. When we have $V_{ext} < 0$ (forward bias) there should be current flowing through the semiconductor, which is confirmed by the simulation.

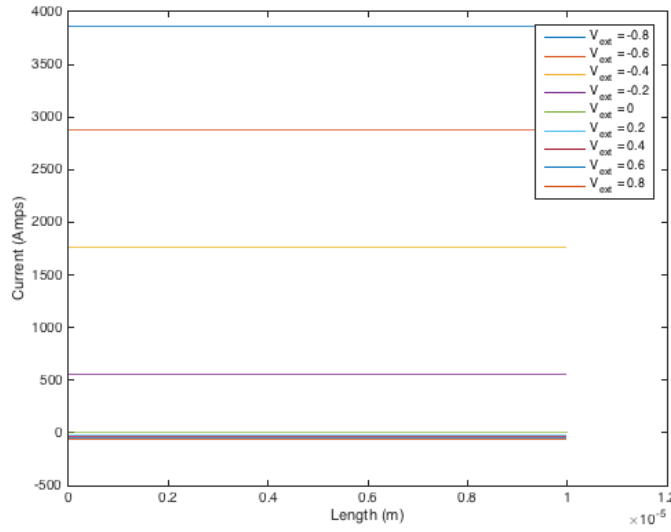


Figure 5.20: The current of doped semiconductor at thermal equilibrium with higher doping in the P-type region.

Figure 5.21 verifies the fact that when we have our PN junction in a forward bias setup ($V_{ext} < 0$), there is little to no current. However, when we have our PN junction in a reverse bias set up ($V_{ext} > 0$), there is current running through the device.

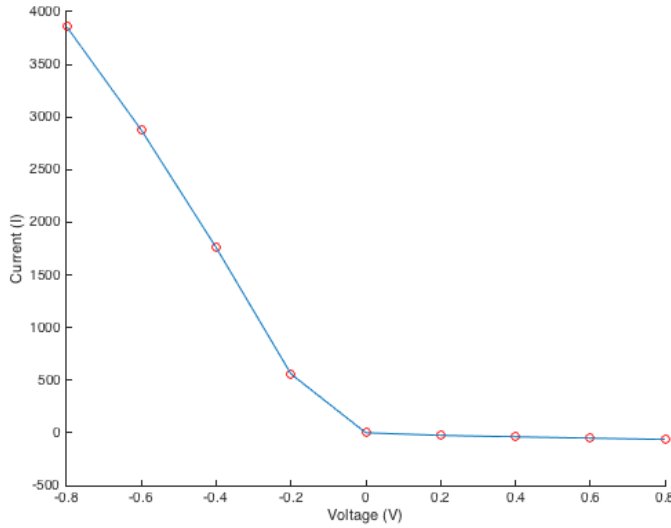


Figure 5.21: The current-voltage plot for different external voltages of doped semiconductor at thermal equilibrium with higher doping in the P-type region.

We now illustrate the results of the simulation of a semiconductor with more doping in the N-type region ($N_A = -10^{16}$, $N_D = 10^{18}$), zero initial potential, and varying external voltage.

Figures 5.22-5.28 are very similar to Figures 5.8-5.14 and Figures 5.15-5.21.

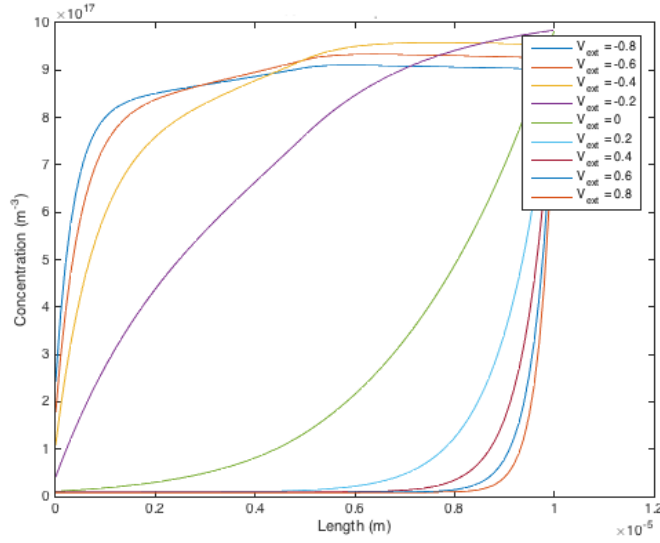


Figure 5.22: Electron concentration of doped semiconductor at thermal equilibrium with higher doping in the N-type region.

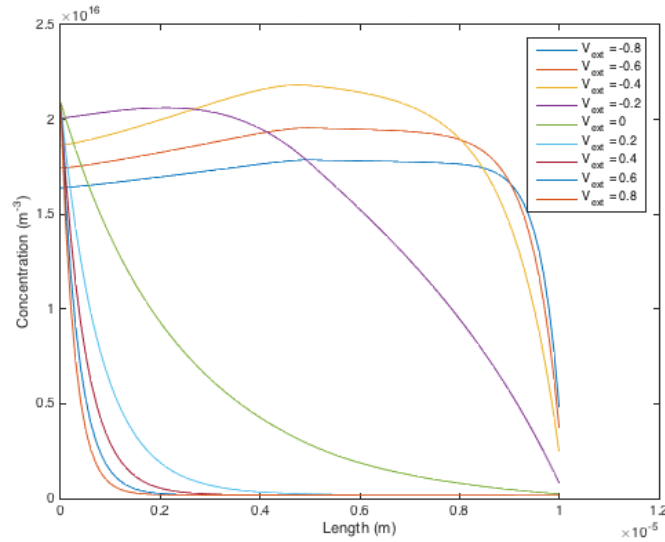


Figure 5.23: Hole concentration of doped semiconductor at thermal equilibrium with higher doping in the N-type region.

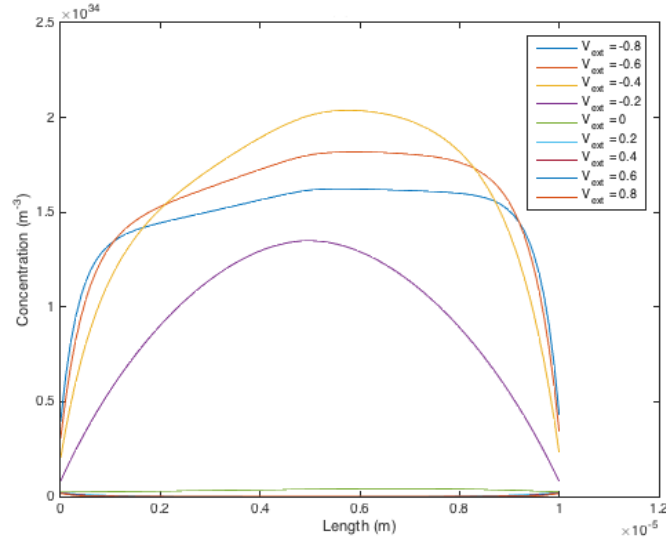


Figure 5.24: Product of electron and hole concentration of doped semiconductor at thermal equilibrium with higher doping in the N-type region.

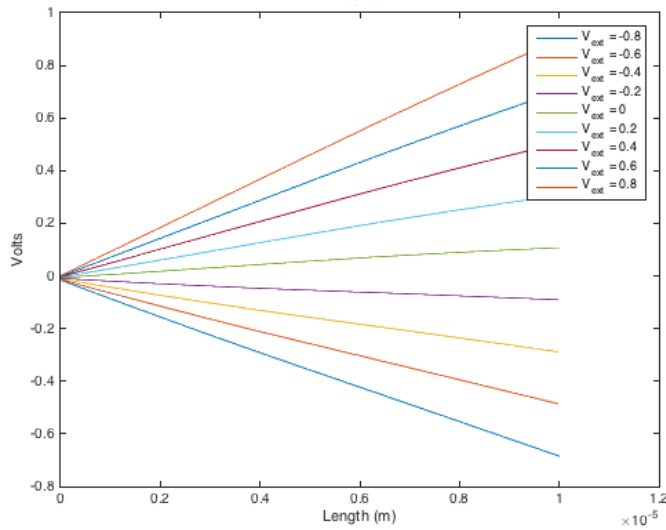


Figure 5.25: Potential of doped semiconductor at thermal equilibrium with higher doping in the N-type region.

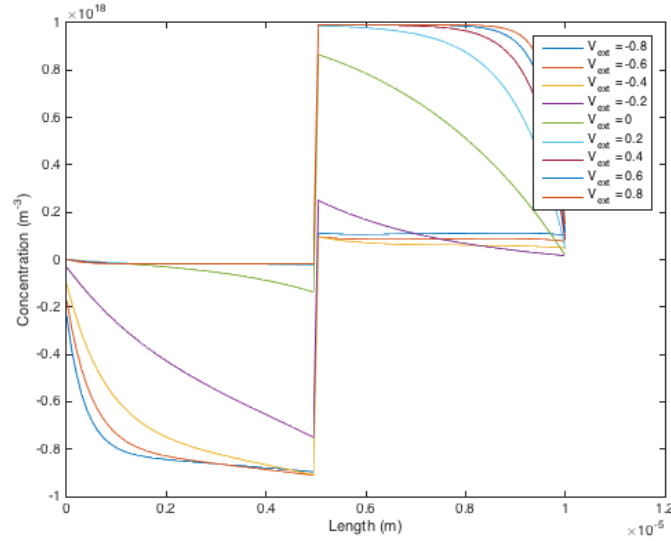


Figure 5.26: The density of doped semiconductor at thermal equilibrium with higher doping in the N-type region.

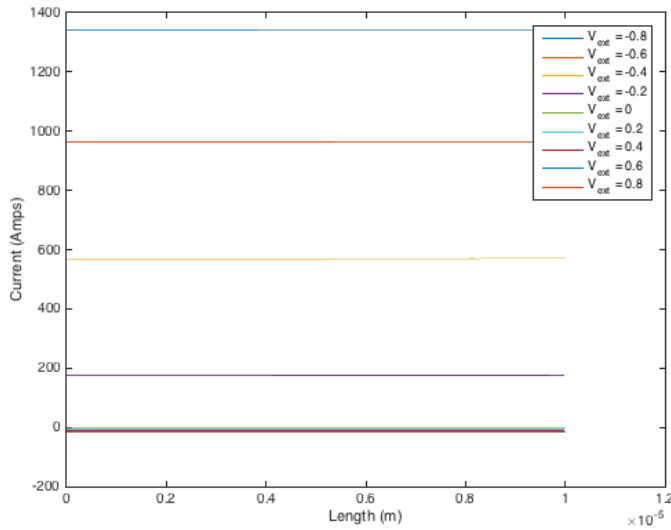


Figure 5.27: The current of doped semiconductor at thermal equilibrium with higher doping in the N-type region.

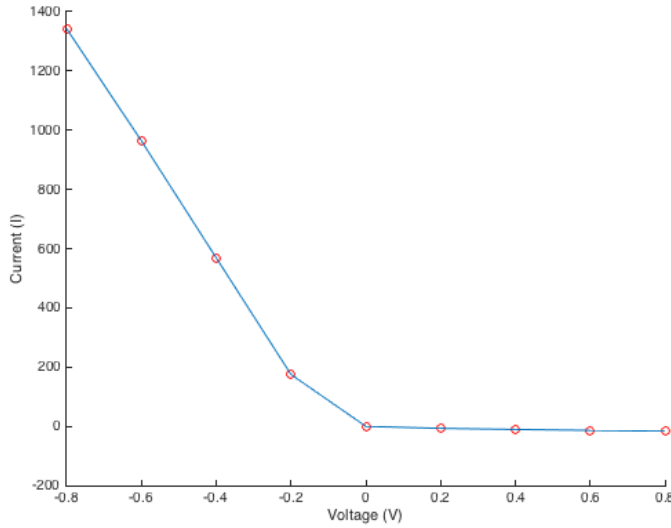


Figure 5.28: The current-voltage plot for different external voltages of doped semiconductor at thermal equilibrium with higher doping in the N-type region.

Focusing on the IV plots in Figures 5.14, 5.21, and 5.28 we confirm that when our PN junction is hooked up with forward bias ($V_{ext} < 0$), we have current flow and when our PN junction is hooked up with a reverse bias ($V_{ext} > 0$), we have no current flow. In other words, under forward bias our depletion region shrinks and under reverse bias our depletion region expands.

CHAPTER 6

SLOTBOOM AND SCHARFETTER-GUMMEL

The ultimate goal of this paper is to compare and contrast Slotboom and the Scharfetter-Gummel flux functions given by $\mathcal{B}_{SB}(x) = \exp(-\frac{x}{2})$ and $\mathcal{B}_{SG}(x) = \frac{x}{\exp(x)-1}$, respectively. In order to compare these two functions and their solutions, we will consider the IV curves with varying amounts of spatial points. We will only consider and analyze the case in which we have zero doping and equal amounts of doping.

6.1 Zero Doping

Figures 6.1 and 6.2 show IV curves using different numbers of spatial points using the Slotboom and Scharfetter-Gummel flux functions for a semiconductor with zero doping.

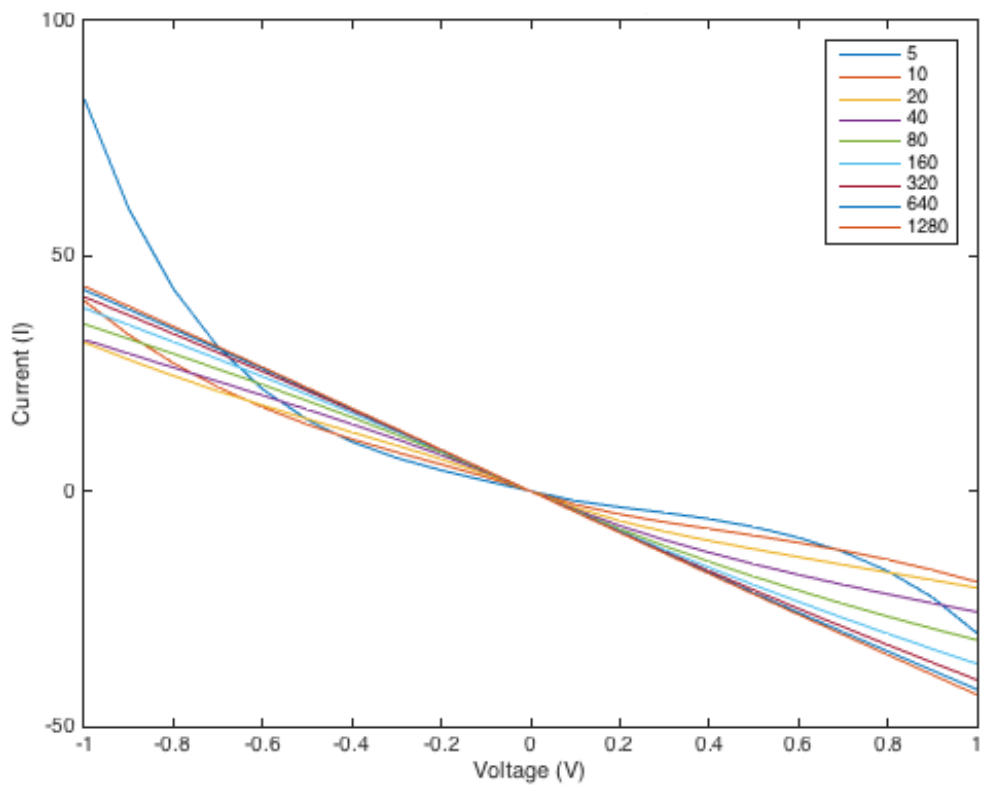


Figure 6.1: Slotboom with zero doping using different numbers of spatial points.

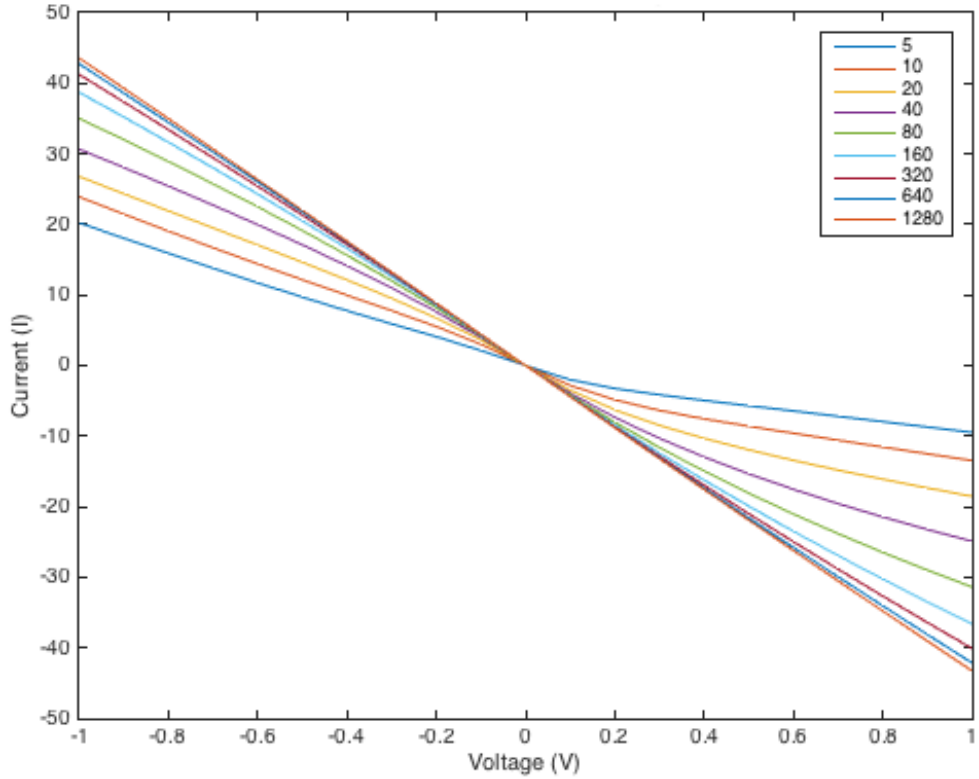


Figure 6.2: Scharfetter-Gummel with zero doping using different numbers of spatial points.

In Figure 6.1, it can be seen that in the case of a large forward bias ($V_{ext} = -1$) and small number of spatial points, the Slotboom flux function is far from the solutions with larger amounts of spatial points. If we look at the Scharfetter-Gummel flux function, the solutions for different numbers of spatial points converge as the spatial points increase. That is to say, the Slotboom flux function discretization starts to diverge in cases of large forward and reverse bias when using a small number of grid points. This phenomenon is related to how \mathcal{B}_{SB} deviates from \mathcal{B}_{SG} in Figure 4.1. For our purposes, we will call the IV curve with

1280 points the refined solution. We can conclude that in this case, the Scharfetter-Gummel flux function better approximates the solution in cases of large forward and reverse bias where the Slotboom flux function diverges from a refined solution. It is important to point out that using a small numbers of spatial points, such as 5 or 10, is extremely uncommon. As we increase the number of spatial points, the IV curves using Scharfetter-Gummel and Slotboom flux functions begin to converge to the refined solution as expected. Figures 6.3-6.6 show the differences in using the Scharfetter-Gummel and Slotboom flux functions compared to the refined solution.

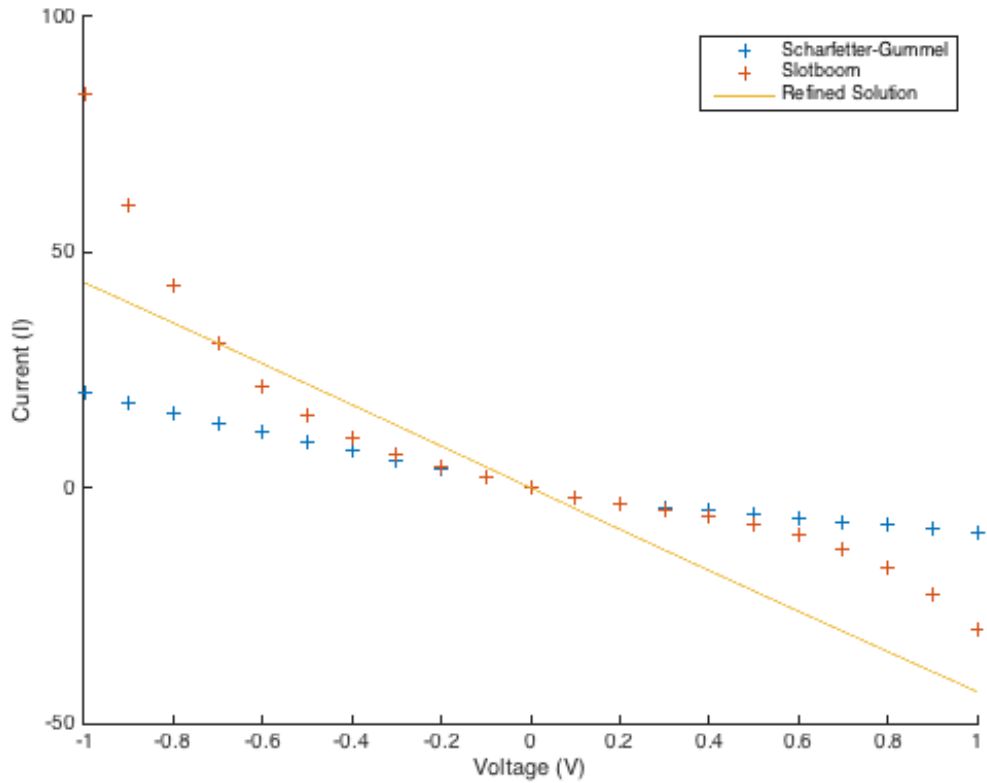


Figure 6.3: Scharfetter-Gummel vs. Slotboom with zero doping using 5 spatial points.

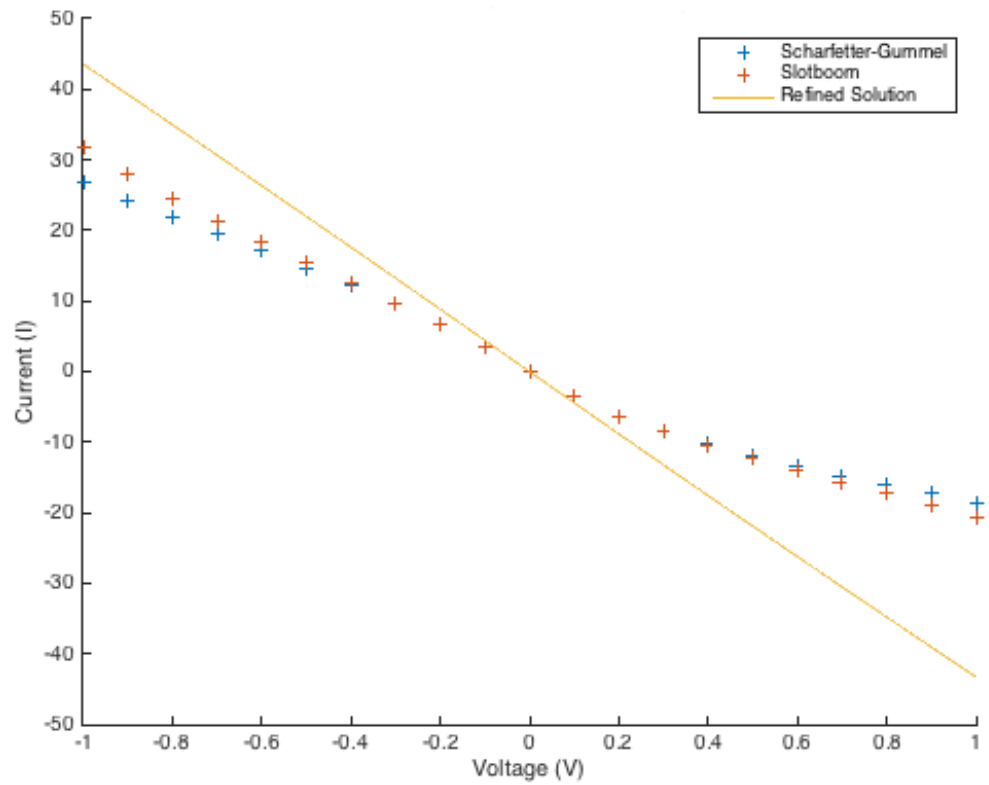


Figure 6.4: Scharfetter-Gummel vs. Slotboom with zero doping using 20 spatial points.

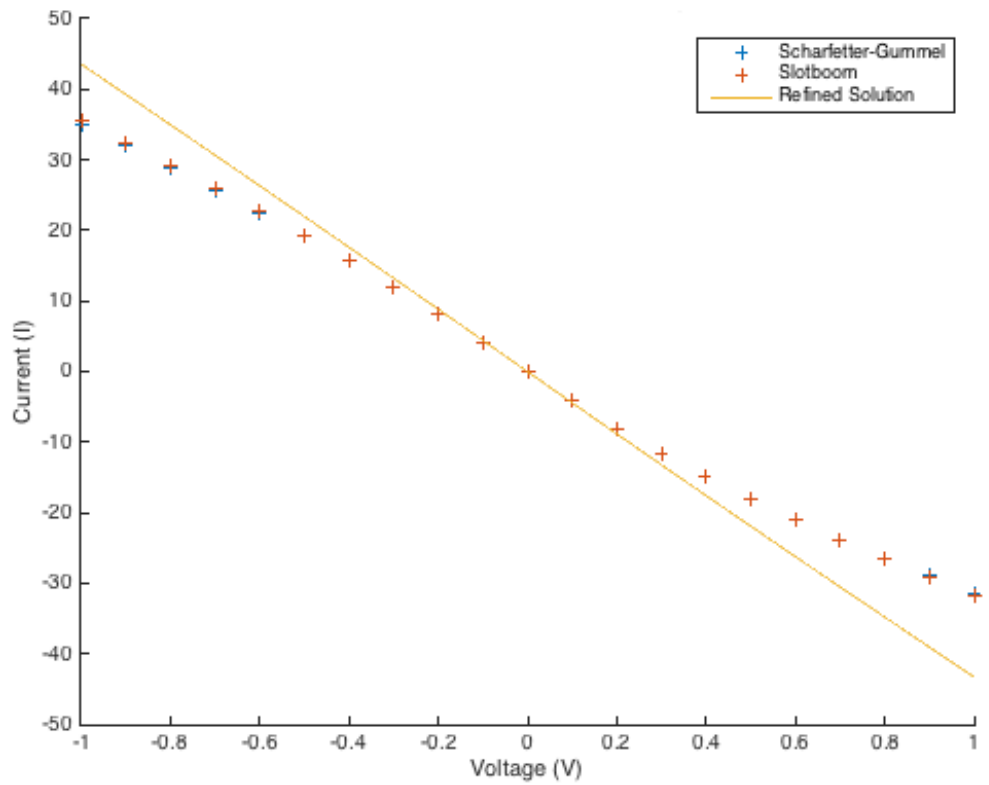


Figure 6.5: Scharfetter-Gummel vs. Slotboom with zero doping using 80 spatial points.

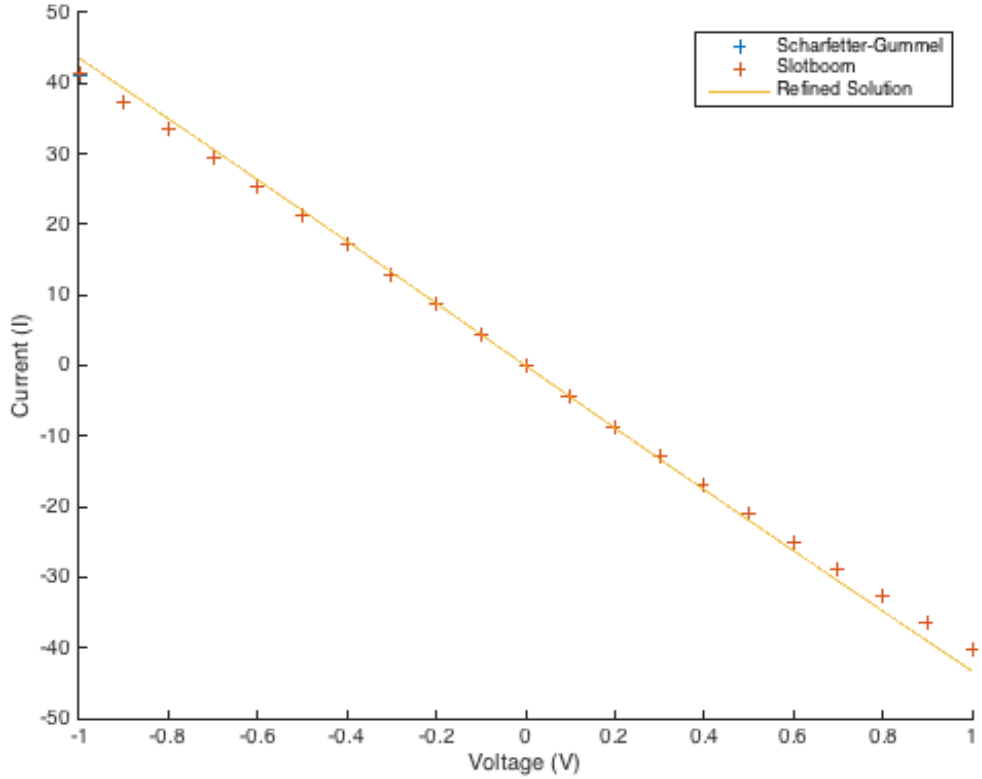


Figure 6.6: Scharfetter-Gummel vs. Slotboom with zero doping using 320 spatial points.

6.2 Equal Doping

Similar to the previous section, now we will look at the case where we have an equal amount of doping ($10^{18} m^{-3}$) and compare the Scharfetter-Gummel and Slotboom flux functions. Figures 6.7 and 6.8 show IV curves using different numbers of spatial points using the Slotboom and Scharfetter-Gummel flux functions for an equally doped semiconductor.

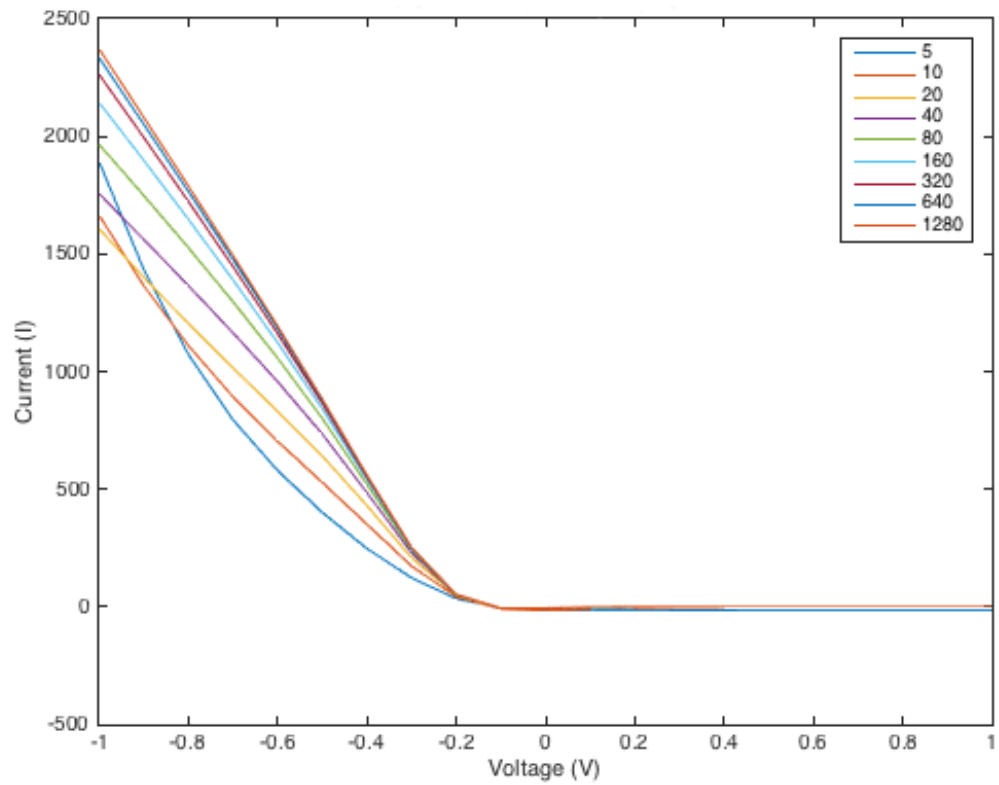


Figure 6.7: Slotboom with an equal amount of doping using different number of spatial points.

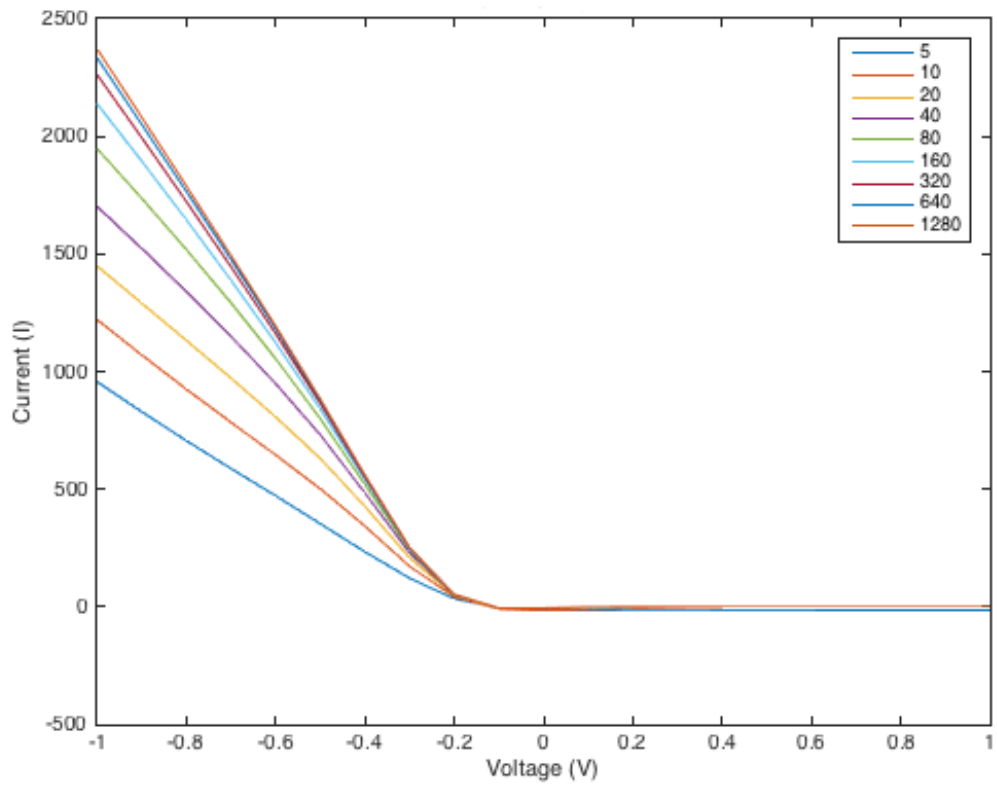


Figure 6.8: Scharfetter-Gummel with an equal amount of doping using different number of spatial points.

Figures 6.9-6.12 show the differences in using the Scharfetter-Gummel and Slotboom flux functions compared to the refined solution.

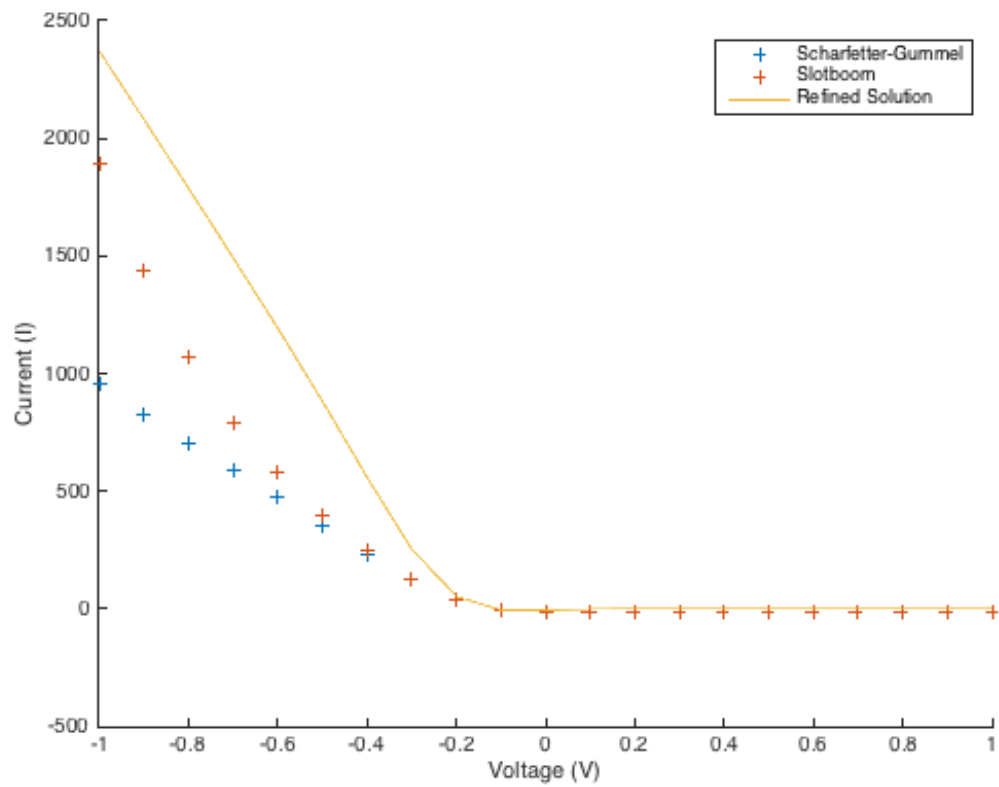


Figure 6.9: Scharfetter-Gummel vs. Slotboom with equal doping using 5 spatial points.

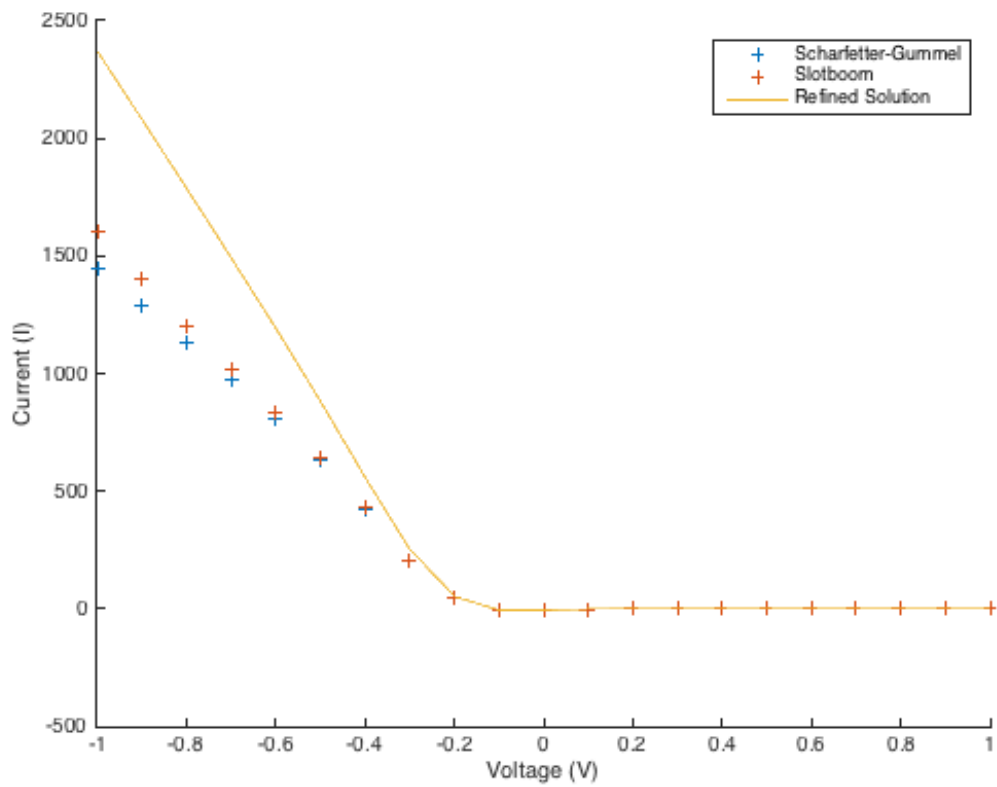


Figure 6.10: Scharfetter-Gummel vs. Slotboom with equal doping using 20 spatial points.

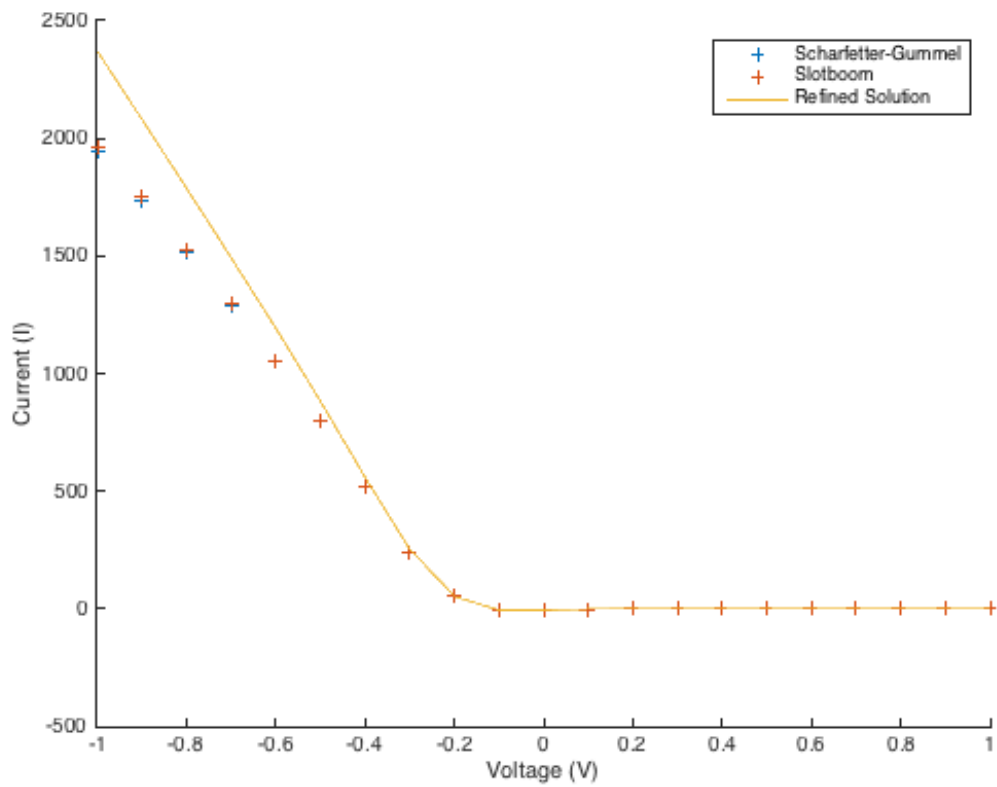


Figure 6.11: Scharfetter-Gummel vs. Slotboom with equal doping using 80 spatial points.

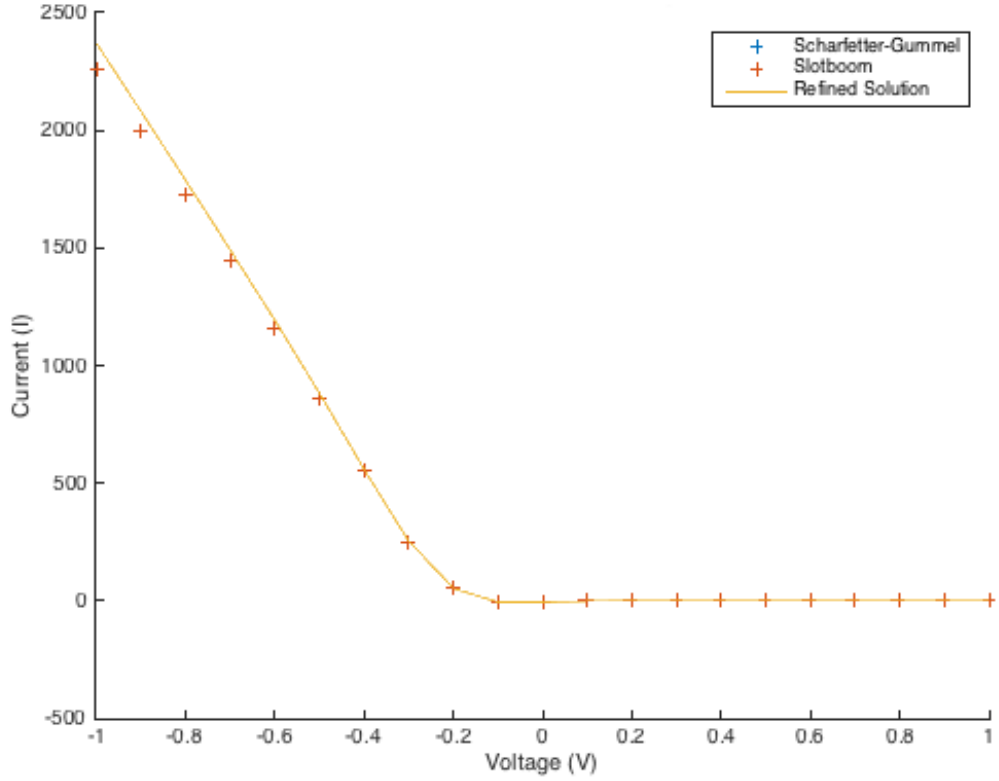


Figure 6.12: Scharfetter-Gummel vs. Slotboom with equal doping using 320 spatial points.

We can see that both functions \mathcal{B}_{SG} and \mathcal{B}_{SB} converge towards this refined solution as we increase the number of spatial points used. However, \mathcal{B}_{SB} converges quicker to the solution. We can also see regardless of which function we use, in the case of reverse bias for an equal amount of doping; our approximations are very close to zero. This reflects that there is no current through the semiconductor in reverse bias. In that case, Scharfetter-Gummel and Slotboom give very accurate approximations to that of the refined solution. The only discrepancies arise are in the case of forward bias when we have current in the semiconductor.

CHAPTER 7

SOLAR CELL

The effects of global climate change become increase every year. The use of fossil fuels releases large amounts of carbon dioxide into the atmosphere, leading to detrimental effects on the environment. Judkins and Fulkerson [JF93] point out that a popular alternative to using fossil fuels to power electronic devices is solar energy. A solar cell is a PN junction in which sunlight acts as an external source of energy in order to generate electrical power. Designs of solar cells can be complex, so we will briefly discuss an application of semiconductors and the Scharfetter-Gummel finite difference scheme.

7.1 Fill Factor

De Vos [Vos83] defines the fill factor as a measure of the quality of a solar cell that is defined as the ratio of the optimal obtainable power to the product of the open-circuit voltage and short-circuit current

$$FF = \frac{P_{opt}}{V_{SC}V_{OC}} = \frac{I_{opt}V_{opt}}{V_{SC}V_{OC}} \quad (7.1)$$

Engineers seek to maximize the fill factor through different designs and parameters. As stated by Colinge and Colinge [CC06], the larger the fill factor, the larger the energy conversion rate of the solar cell.

In order to find the fill factor of a solar cell, we will make use of the IV curves in Chapter 6. To simulate light generation, we will shift our refined IV curve down for the equal doping case by some constant. There are more rigorous ways to include a

light generation term, G , but we will not consider them for this paper. In order to find P_{opt} , V_{SC} , and V_{OC} we will use interpolation and an intersection technique found in Burden and Faires [BF11] and Stoer and Bulirsch [SB80], which can be found in Appendix A.

Figures 7.1 and 7.2 show graphs of shifted IV curves.

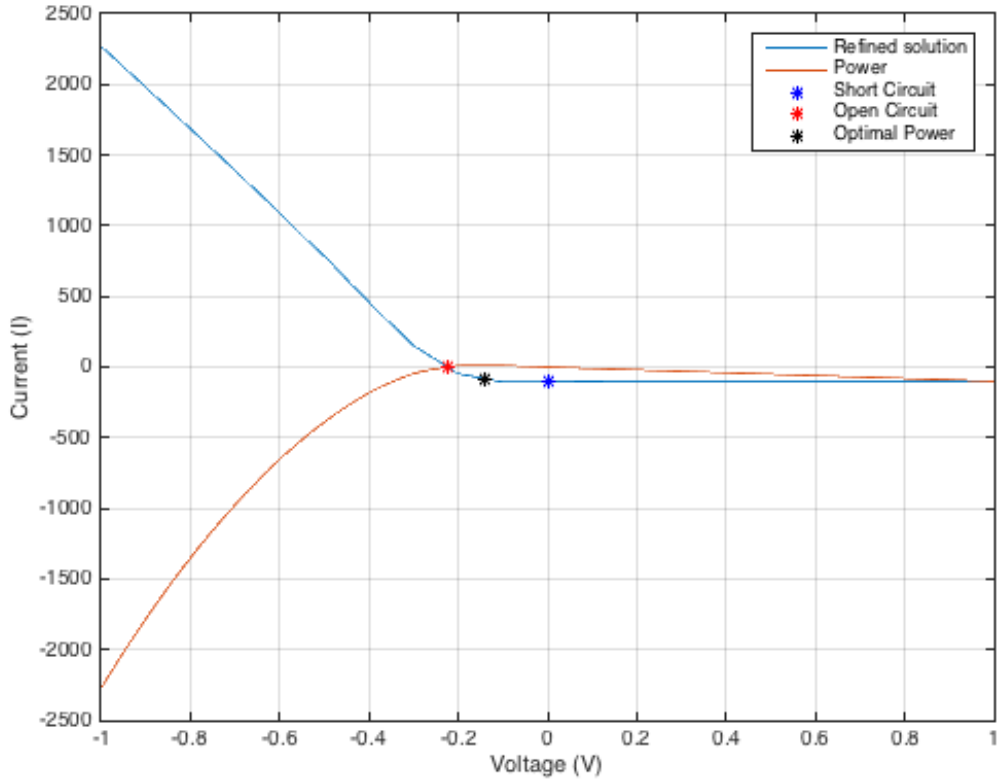


Figure 7.1: IV curve and power curve of a solar cell with a shift of 100.

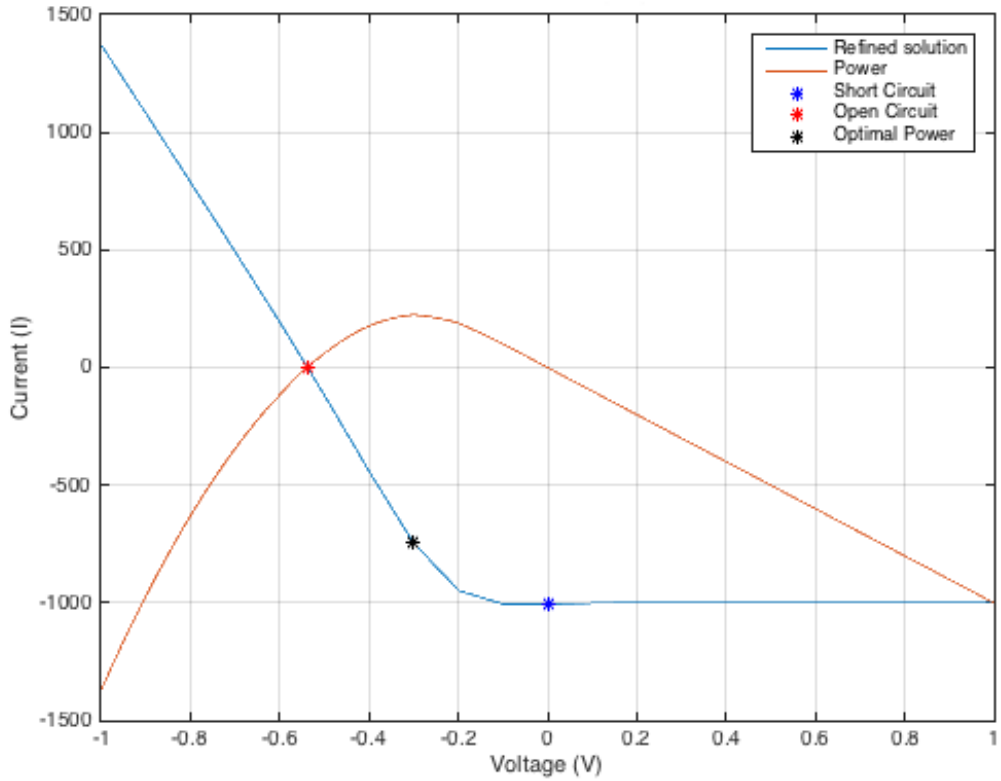


Figure 7.2: IV curve and power curve of a solar cell with a shift of 1000.

7.2 Future Work

We will not conclude that the fill factor is accurate for a silicon solar cell with our parameters, but will note that Figures 7.1 and 7.2 agree with what one would expect. Calculating the fill factor for the two scenarios above, we obtain 0.4898 and 0.4147, respectively, while typical fill factors range from 0.5 to 0.8 [Fil12]. Both flux functions calculate these fill factors with small relative error. The above only sets up a framework of what can be done using the Scharfetter-Gummel finite difference scheme and different flux functions. Future work will consist of using better parameters to model a realistic solar cell with a fill factor $> 80\%$.

BIBLIOGRAPHY

- [ARS97] U.M. Ascher, S.J. Ruuth, and R.J. Spiteri, *Implicit-explicit runge-kutta methods for time-dependent partial differential equation*.
- [BD77] W.E. Boyce and R.C. DiPrima, *Elementary differential equations*, Wiley & Sons, 1977.
- [BF11] R.L. Burden and J.D. Faires, *Numerical analysis*, Brooks/Cole, 2011.
- [BK50] G.G. O' Brien and M.A. Kaplan, *A study of the numerical solution of partial differential equations*, Journal of Mathematics and Physics **29** (1950).
- [Bri12] D. Brinkman, *Modeling and numerics for two partial differential equation systems arising from nanoscale physics*, 2012.
- [CC06] J. Colinge and C. Colinge, *Physics of semiconductor devices*, Springer, 2006.
- [CN47] J. Crank and P. Nicolson, *A practical method for numerical evaluation of solutions of partial differential equations of the heat-conduction type*, Mathematical Proceedings of the Cambridge Philosophical Society (1947).
- [Eva15] L. Evans, *Partial differential equations*, 3rd ed., American Mathematical Society, 2015.
- [Fil12] *Photovoltaic cell i-v characterization theory and labview analysis code - national instruments*, <http://www.ni.com/white-paper/7230/en/>, 2012.
- [FRD⁺16] P. Farrell, N. Rotundo, D.H. Doan, M. Kantner, J. Fuhrmann, and T. Koprucki, *Numerical methods for drift-diffusion models*.
- [Gum64] H.K. Gummel, *A self-consistent iterative scheme for one-dimensional steady state transistor calculations*, IEEE Transactions on Electron Devices (1964), 455–465.
- [JF93] R.R. Judkins and W. Fulkerson, *The dilemma of fossil fuel use and global climate change*, Energy Fuels (1993), no. 7, 14–22.

- [Lev07] R. J. Leveque, *Finite difference methods for ordinary and partial differential equations*, Society for Industrial and Applied Mathematics, 2007.
- [LR56] P. D. Lax and R. D. Richtmyer, *Survey of the stability of linear finite difference equations*, Comm. Pure Appl. Math (1956), no. 9, 267–293.
- [LT09] S. Larsson and V. Thomée, *Partial differential equations with numerical methods*, Springer-Verlag, 2009.
- [Mar86] P.A. Markowich, *The stationary semiconductor device equations*, Springer, 1986.
- [MRS90] P. A. Markowich, C. A. Ringhofer, and C. Schmeiser, *Semiconductor equations*, Springer, 1990.
- [RDM55] Richtmyer R. D. and K. W. Morton, *Difference methods for initial-value problems*, Interscience Publishers, 1955.
- [SA15] M. S. Silberberg and P. Amateis, *Chemistry: The molecular nature of matter and change*, McGraw Hill Education, 2015.
- [SB80] J. Stoer and R. Bulirsch, *Introduction to numerical analysis*, Springer-Verlag, 1980.
- [Sel84] S. Selberherr, *Analysis and simulation of semiconductor devices*, Springer, 1984.
- [SG69] D.L. Scharfetter and H.K. Gummel, *Large-signal analysis of a silicon read diode oscillator*, IEEE Transactions on Electron Devices (1969).
- [Shi50] W. Shiockley, *Electrons and holes in semiconductors*, D. Van Nostrand Company, Inc., 1950.
- [Slo73] J.W. Slotboom, *Computed-aided two dimensional analysis of bipolar transistors*, IEEE Transactions on Electron Devices (1973).
- [Smi73] G.D. Smith, *Numerical solution of partial differential equations: Finite difference methods*, Oxford University Press, 1973.
- [VG06] D. Vasileska and S. Goodnick, *Computational electronics*, Morgan & Claypool Publishers, 2006.
- [Vos83] A. De Vos, *The fill factor of a solar cell from a mathematical point of view*, Solar Cells (1983).

- [vR50] W. van Roosbroeck, *Theory of the flow of electrons and holes in germanium and other semiconductors*, Bell System Technical Journal **29** (1950), 560–607.

APPENDIX A

MATLAB CODE

A.1 Implicit Drift-Diffusion Equation Solver

```
%Drift-Diffusion Equation 1 in one dimension u_t = Du_xx - vu_x
%Forward time forward space (FTBS) with Periodic Boundary Conditions
%Implicit Scheme
%Sinusoidal potential

k = 0.1; %time size
h = 0.1; %step size
J = 101; %number of steps
I = 200; %number of time steps
R2 = k./h^2;
R1 = k./h;
D = 0.1; %diffusion coefficient
N = 2*pi/(J-1)/h; %Normalization factor
x = [0:h:(J-1)*h]; %vector
V = (1/N).* diff(cos(N.*(x-5)))./h; %del potential vector
V(J) = V(1);

%Boundary conditions
```

```

a = 0;
u_original(1,1) = a;
u_original(J,1) = a;

u_original(:,1) = exp(-(x-5).^2);

u_new(1,:) = u_original;

for k = 1:I

%Find all velocities in each spatial position
for l = 1:J
v_original(l,:)= -V;
end

%Creating the matrix A
if v_original(1,1) > 0
A(1,1) = 1+2.*D.*R2 + v_original(1,1);
else
A(1,1) = 1+2.*D.*R2 - v_original(1,1);
end

if v_original(1,2) > 0
A(1,2) = -D.*R2;
else
A(1,2) = v_original(1,2).*R1 - D.*R2;
end

```

```

end

for i = 2:J-1
if v_original(i,i-1) > 0
A(i,i-1) = -v_original(i,i-1).*R1 - D.*R2;
else
A(i,i-1) = -D.*R2;
end

if v_original(i,i) > 0
A(i,i) = 1+2.*D.*R2 + v_original(i,i);
else
A(i,i) = 1+2.*D.*R2 - v_original(i,i);
end

if v_original(i,i+1) > 0
A(i,i+1) = -D.*R2;
else
A(i,i+1) = v_original(i,i+1).*R1 - D.*R2;
end
end

if v_original(J,J-1) > 0
A(J,J-1) = -v_original(J,J-1).*R1 - D.*R2;
else
A(J,J-1) = -D.*R2;
end

```

```
if v_original(J,J) > 0
A(J,J) = 1+2.*D.*R2 + v_original(J,J);
else
A(J,J) = 1+2.*D.*R2 - v_original(J,J);
end
```

```
%Boundary conditions
```

```
if v_original(1,J) > 0
A(1,J) = -v_original(1,J) - D.*R2 ;
else
A(1,J) = -D.*R2;
end
if v_original(J,1) > 0
A(J,1) = -D.*R2 ;
else
A(J,1) = v_original(J,1)-D.*R2;
end
u_new(k+1,:) = A\u_new(k,:);
```

A.2 Scharfetter-Gummel Finite Difference Scheme

```
% Scharfetter-Gummel Finite Difference Scheme

%Physical constants
mu_n = 0.14; %electron mobility
mu_p = 0.045; %hole mobility
k_B = 1.38064852e-23; %Boltzmann constant
temp = 300; %temperature
q = 1.602e-19; %elementary charge
V_T = k_B * temp / q; %thermal voltage
eps_0 = 8.854187817e-12; %permittivity of free space
eps_s = 11.86; %dielectric constant of silicon
eps = eps_s*eps_0; %permittivity of silicon
n_i = 1.5e16; %intrinsic concentration
N_D = 1e18; %donor concentration
N_A = -1e18; %acceptor concentration
tau_n = 1e-6; %electron life time
tau_p = 1e-5; %hole life time

%Finite differences
L = 100; %L spatial points
LL = 1e-5; %length of device
T = 500; %number of time iterations
TT = 1e-8; %total time elapsed
dx = LL/(L-1); %spatial step
```

```

dt = TT/T;                                %temporal step
x = [0:dx:LL];                            %spatial vector

%Doping profile
CC = [N_A*ones(1,floor(L/2)) N_D*ones(1,ceil(L/2))];
con_n = dt*V_T*mu_n/dx^2;
con_p = dt*V_T*mu_p/dx^2;

%Poisson Matrix
d = [-1 0 1]';
m = [-ones(1,L);2*ones(1,L);-ones(1,L)]';
PM = spdiags(m,d,L,L);

%Ohmic boundary condition vectors
nBCleft = 0.5 * (sqrt(N_A^2 + 4*n_i^2) + N_A);    %BC for electrons
nBCright = 0.5 * (sqrt(N_D^2 + 4*n_i^2) + N_D);   %BC for electrons
pBCleft = 0.5 * (sqrt(N_A^2 + 4*n_i^2) - N_A);    %BC for holes
pBCright = 0.5 * (sqrt(N_D^2 + 4*n_i^2) - N_D);   %BC for holes

%Electric Potential Vector Initialization
V = 0.*x;

%Realistic initial conditions
n(1,:) = [nBCleft*ones(1,floor(L/2)) nBCright*ones(1,ceil(L/2))];
p(1,:) = [pBCleft*ones(1,floor(L/2)) pBCright*ones(1,ceil(L/2))];

```

```

%External Voltage
V_ext = [ -1:0.1:1];

for h = 1:length(V_ext)

%Built in Potential
V.bi_left = V_T*log((N_A + sqrt(N_A^2 + 4*n_i^2)) / (2*n_i));
V.bi_right = V_T*log((N_D + sqrt(N_D^2 + 4*n_i^2)) / (2*n_i))+V_ext(h);
dV = [(V(1) - V.bi_left), diff(V)./V_T, (V.bi_right - V(L))];

%Scharfetter-Gummel Iterations
for k = 1:T

%Gummel Loop
for l = 1:10

%Boundary condition updates
BCn(1) = -con_n*bernofun(-dV(1))*nBCleft;
BCn(L) = -con_n*bernofun(dV(L))*nBCright;
BCp(1) = -con_p*bernofun(dV(1))*pBCleft;
BCp(L) = -con_p*bernofun(-dV(L))*pBCright;
BCV(1) = V.bi_left; BCV(L) = V.bi_right;

%First row electrons and holes

```

$N(1,1) = \text{bernfun}(-dV(2)) + \text{bernfun}(dV(1));$

$N(1,2) = -\text{bernfun}(dV(2));$

$P(1,1) = \text{bernfun}(dV(2)) + \text{bernfun}(-dV(1));$

$P(1,2) = -\text{bernfun}(-dV(2));$

%Reaction terms Shockley–Read–Hall

$IN(1,1) = 1 + mm * (dt.*p(k,1))./(tau_n.(n(k,1)+n_i)) +$
 $\tau_{au_p}.*(p(k,1)+n_i));$

$IP(1,1) = 1 + mm * (dt.*n(k,1))./(tau_n.(n(k,1)+n_i)) +$
 $\tau_{au_p}.*(p(k,1)+n_i));$

$c_int(1) = (-n_i^2.*dt)./(tau_n.(n(k,1)+n_i)) + \tau_{au_p}.*(p(k,1)+n_i));$

%Current

$J_n(k,1) = (q*mu_n*V_T/dx).*(\text{bernfun}(dV(1))*n(k,1) -$
 $\text{bernfun}(-dV(1))*nBCleft);$

$J_p(k,1) = (q*mu_p*V_T/dx).*(\text{bernfun}(-dV(1))*p(k,1) -$
 $\text{bernfun}(dV(1))*pBCleft);$

for j = 2:L

$J_n(k,j) = (q*mu_n*V_T/dx).*(\text{bernfun}(dV(j))*n(k,j) -$
 $\text{bernfun}(-dV(j))*n(k,j-1));$

$J_p(k,j) = (q*mu_p*V_T/dx).*(\text{bernfun}(-dV(j))*p(k,j) -$
 $\text{bernfun}(dV(j))*p(k,j-1));$

end

%Iterate through rows (2:L) electrons and holes

```

for j = 2:L-1
N(j,j-1) = -bernofun(-dV(j));
N(j,j) = bernofun(-dV(j+1)) + bernofun(dV(j));
N(j,j+1) = -bernofun(dV(j+1));
P(j,j-1) = -bernofun(dV(j));
P(j,j) = bernofun(dV(j+1)) + bernofun(-dV(j));
P(j,j+1) = -bernofun(-dV(j+1));
IN(j,j) = 1 + mm*(dt.*n(k,j))./(tau_n.* (n(k,j)+n_i)) +
tau_p.* (p(k,j)+n_i));
IP(j,j) = 1 + mm*(dt.*p(k,j))./(tau_n.* (n(k,j)+n_i)) +
tau_p.* (p(k,j)+n_i));
c_int(j) = (-n_i.^2.*dt)./(tau_n.* (n(k,j)+n_i)) + tau_p.* (p(k,j)+n_i));
end

%Last row (L) electrons and holes
N(L,L-1) = -bernofun(-dV(L));
N(L,L) = bernofun(dV(L+1)) + bernofun(dV(L));
P(L,L-1) = -bernofun(dV(L));
P(L,L) = bernofun(-dV(L+1)) + bernofun(-dV(L));

%Reaction terms Shockley–Read–Hall
IN(L,L) = 1 + mm*(dt.*p(k,L))./(tau_n.* (n(k,L)+n_i)) +
tau_p.* (p(k,L)+n_i));
IP(L,L) = 1 + mm*(dt.*n(k,L))./(tau_n.* (n(k,L)+n_i)) +
tau_p.* (p(k,L)+n_i));

```

$c_int(L) = (-n_i.^2.*dt)./(tau_n.*(\mathbf{n}(k,L)+n_i) + tau_p.*(\mathbf{p}(k,L)+n_i));$

$N = \text{con_n}.*N;$

$P = \text{con_p}.*P;$

$\mathbf{n}(k+1,:) = (\mathbf{IN} + N)\backslash(\mathbf{n}(k,:)) - BCn - c_int';$

$\mathbf{p}(k+1,:) = (\mathbf{IP} + P)\backslash(\mathbf{p}(k,:)) - BCp - c_int';$

$U = (dx^2.*q./\text{eps}).*(\mathbf{p}(k+1,:)) - \mathbf{n}(k+1,:) + CC + BCV;$

$V_new = (PM\backslash U');$

$V = V_new;$

$dV = [(V(1) - V_bi_left), \text{diff}(V)./V_T, (V_bi_right - V(L))];$

end

end

$J = J_n(end,:)$ – $J_p(end,:);$

$\text{current}(h,:)$ = $J;$

$MJ(h) = \min(J);$

$\text{potential}(h,:)$ = $V_new;$

$\text{density}(h,:)$ = $CC + p(end,:)$ – $n(end,:);$

$\text{electrons}(h,:)$ = $n(end,:);$

$\text{holes}(h,:)$ = $p(end,:);$

end

A.3 Flux Functions

```
% The Flux Function
function B = bernfun(x)
tol = 1e-10;
% Slotboom
B = exp(-x./2);
%Scharfetter-Gummel
if abs(x) <= tol
B = 1;
else
B = x./ (exp(x) - 1);
end
```

A.4 Solar Cell and Fill Factor

```
%Post Processing graphs of SB and SG
%Fill Factor of solar cell

load('PostProcessingAll3.mat')
shift = 100; %Light generation
lin_V = [-1:0.001:1];

figure
for i = 1:size(SBPP,1)
    interSBPP = interp1(V_ext,SGPP(i,:),lin_V);
    interSGPP = interp1(V_ext,SBPP(i,:),lin_V);
    plot(lin_V,interSGPP,lin_V,interSBPP)
    title('Scharfetter-Gummel vs. Slotboom Zero Doping')
    xlabel('Voltage (V)')
    ylabel('Current (I)')
    legend('Scharfetter-Gummel','Slotboom')
    hold off
end

for i = 1:size(SBPP18)
    figure
    scatter(V_ext, SGPP18(i,:), '+')
    hold on
end
```

```

scatter(V_ext, SBPP18(i,:), '+')
hold on
plot(lin_V,interSGPP18(end,:))
title('Scharfetter-Gummel vs. Slotboom Equal Doping 1e18')
xlabel('Voltage (V)')
ylabel('Current (I)')
legend('Scharfetter-Gummel','Slotboom','Refined Solution')
end

%Shift interpolated IV plot down
intersolarSB = interSBPP18(end,:)-shift;
intersolarSG = interSGPP18(end,:)-shift;

%Optimal Power max Power = IV
[opt_powSB, idxpowSB] = max(lin_V.*intersolarSB);
[opt_powSG, idxpowSG] = max(lin_V.*intersolarSG);

%Short Circuit at V_ext = 0
SC_SB = intersolarSB(1001);
SC_SG = intersolarSG(1001);

%Open Circuit
y = zeros(1,length(lin_V));
idxSBPP18 = find(intersolarSB-y<eps,1);
idxSGPP18 = find(intersolarSG-y<eps,1);

```

```
OC_SB = lin_V(idxSBPP18);
OC_SG = lin_V(idxSGPP18);

figure
plot(lin_V, intersolarSG, lin_V, lin_V.*intersolarSG)
grid on
hold on
scatter(lin_V(1001), intersolarSG(1001), '*', 'b')
hold on
scatter(lin_V(idxSGPP18), intersolarSG(idxSBPP18), '*', 'r')
hold on
scatter(lin_V(idxpowSG), intersolarSG((idxpowSB)), '*', 'k')
hold on
title('Solar Cell IV Curve')
xlabel('Voltage (V)')
ylabel('Current (I)')
legend('Refined solution', 'Power', 'Short Circuit', 'Open Circuit',
'Optimal Power')

%Fill Factor
FF_SB = opt_powSB / (SC_SB * OC_SB)
FF_SG = opt_powSG / (SC_SG * OC_SG)
```